Table 1 | Lists of gene sets for identifying gene networks.

Category	Set1	Set2	Set3
Pathway signaling		Map2k1	Adora2a
		Mapk1	Drd5
		Mapk3	Fgf13
		Pla2g6	Gnao1
		Rps6ka1	Notch2
		Shc1	Tnr
Transcription/chromatin regulation	RARa	Atbf1	Ascl1
	RARb	Cdyl	Gusb
	RARg	Rhog	Mef2c
	Nanog	Rif1	Pax5
	Pou5f1	Sall1	Pou3f3
	Zfp42	Smarcad1	
Neural development	Fgfr1	Fos	Bdnf
	Olig2	Gbx2	Gdnf
	Sox2	Hras1	Nrp2
		Raf1	Slit2
		Sox2	Ywhah
Neural marker	Gfap	Gfap	Gfap
	Map2	Map2	Map2
	Nestin	Nestin	Nestin
	Tuj1	Tuji1	Tuji1

GENE INTERACTION ANALYSIS

Matrices transferred from gene interaction analysis for set 1, set 2, and set 3 are shown in **Figures 3–5**, respectively (see **Figures A1–A3** in Appendix as references and Tables S1–S6 in Supplementary Material for input data and output raw-results). In the control group of set 1, *Nanog*, and Sox2 (**Figure 3**) which control ESC pluripotency, regulate many other genes on DoD 0, 2, and 8. On DoD 36, Sox2 does not regulate any gene. In RA-treated groups of set 1, linkages of RARs in the matrix indicated that these genes might play principal roles in the regulation of expression of other genes. Briefly, the effect of RA was observed on DoD 8, in which RA 10^{-8} or 10^{-7} M aggravated *Nanog* and *Pou5f1*. On DoD 36, the matrix was more strongly influenced by RA, in which the neural marker genes such as *Gfap* and *Map2* up-regulated the other genes, indicating that RA enhances neural differentiation (**Figure 3**).

Gene interaction matrix analysis for set 2 is shown in **Figure 4**. In the mESC matrix, linkages between genes were concentrated to categories of pathway signaling and neural development, which is similar with those in set 1 on DoD 8 and DoD 36. It is noteworthy that Gbx2 as a neuronal development marker strongly up-regulated *Mapk3*, *Atbf1*, *Rhog*, *Sall1*, *Smarcad*, *Sox2*, and *Map2* on DoD 8 as well as DoD 36 in RA 10^{-8} M matrices. RA-treated matrices showed that linkages shifted to the right side of the matrix with increasing RA concentrations. Finally, linkages on DoD 36 were concentrated to categories of neural development and neural markers.

Gene interaction network analysis for set 3 is shown in **Figure 5**. In the mESC matrix, linkages between genes were concentrated to transcription/chromatin regulation and pathway signaling categories. Linkages between genes in the control matrix on DoD 8 were concentrated to pathway signaling and neural development categories. In the RA-treated matrices, linkages between genes moved to the neural marker category from the neural development category in a dose-dependent manner. Most of the linkages between genes in the RA-treated matrices on DoD 36 were concentrated to pathway signaling and neural marker categories, suggesting that *Gfap* mainly regulates neuronal differentiation.

DISCUSSION

In the present study, a prediction model for the neural differentiation of mESCs was established and stage-specific gene expression signatures in response to RA were identified using Bayesian network analysis. Our present findings showed that RA significantly increased the size of neurosphere, neuronal cells, and glial cells on DoD 36. In addition, neural marker *Gfap* remarkably up-regulated the other genes in gene set 1 and 3, and neural development marker *Gbx2* significantly up-regulated the other genes in gene set 2 on DoD 36 in the presence of RA. These findings suggest that our protocol for identification of developmental stage-specific gene expression and interaction is a useful method for the screening of environmental chemical toxicity during neurodevelopmental periods.

RA is known as a severe teratogen and causes central nervous system malformations. However, *in vivo* study indicated that high dose (70 mg/kg body weight; b.w.) of RA could induce teratogenic effects during gestational day 7–9 in Swiss mice (Veiga Quemelo et al., 2007). In addition, it was reported that the physiological dose that cannot affect RAR level was 1 mg/kg b.w. and minimally teratogenic dose was 10 mg/kg b.w. and completely teratogenic dose was 100 mg/kg b.w. in gestational day 9 of mouse (Harnisha et al., 1990). In the present study, we selected the dose of RA as 10^{-8} and 10^{-7} M because endogenous levels of RA-induced neural differentiation in the early embryo are approximately 1–10 nM (Maden et al., 1998; Mic et al., 2003). Therefore, we considered to use 10^{-8} M as a low dose and 10^{-7} M as a high dose to examine the effect of RA on stage-specific gene expression signature in mESCs.

We have also successfully designed a mESC neural differentiation protocol to evaluate the effect of RA on the neural differentiation of mESCs. Morphological analysis using a high-content image analyzer was able to acquire varying differences of differentiation from mESCs to neural cells by the RA treatment. For instance, neuronal or glial differentiation from neuronal ESCs was delayed in control cells without induction by RA, which was further confirmed by the lower expression levels of *Map2* and *Gfap* detected on DoD 36. RA treatments promoted the loss of pluripotency and differentiation into neural ESCs up to DoD 36 in the present study (**Figures 1B,C**), suggesting that the maturation of *Map2*-positive neurons and *Gfap*-positive astrocytes were accelerated by RA treatment. Our results are consistent with a study showing that RA and LIF enhance the induction of *Gfap*-positive astrocytes from mice neural progenitor cells via epigenetic modifications (Asano et al., 2009).

In restricted sample size analysis like the present study, simulations using Bayesian network analysis have been suggested to be a very effective method (Toyoshiba et al., 2006). Our present study provided a new experimental evidence that Bayesian

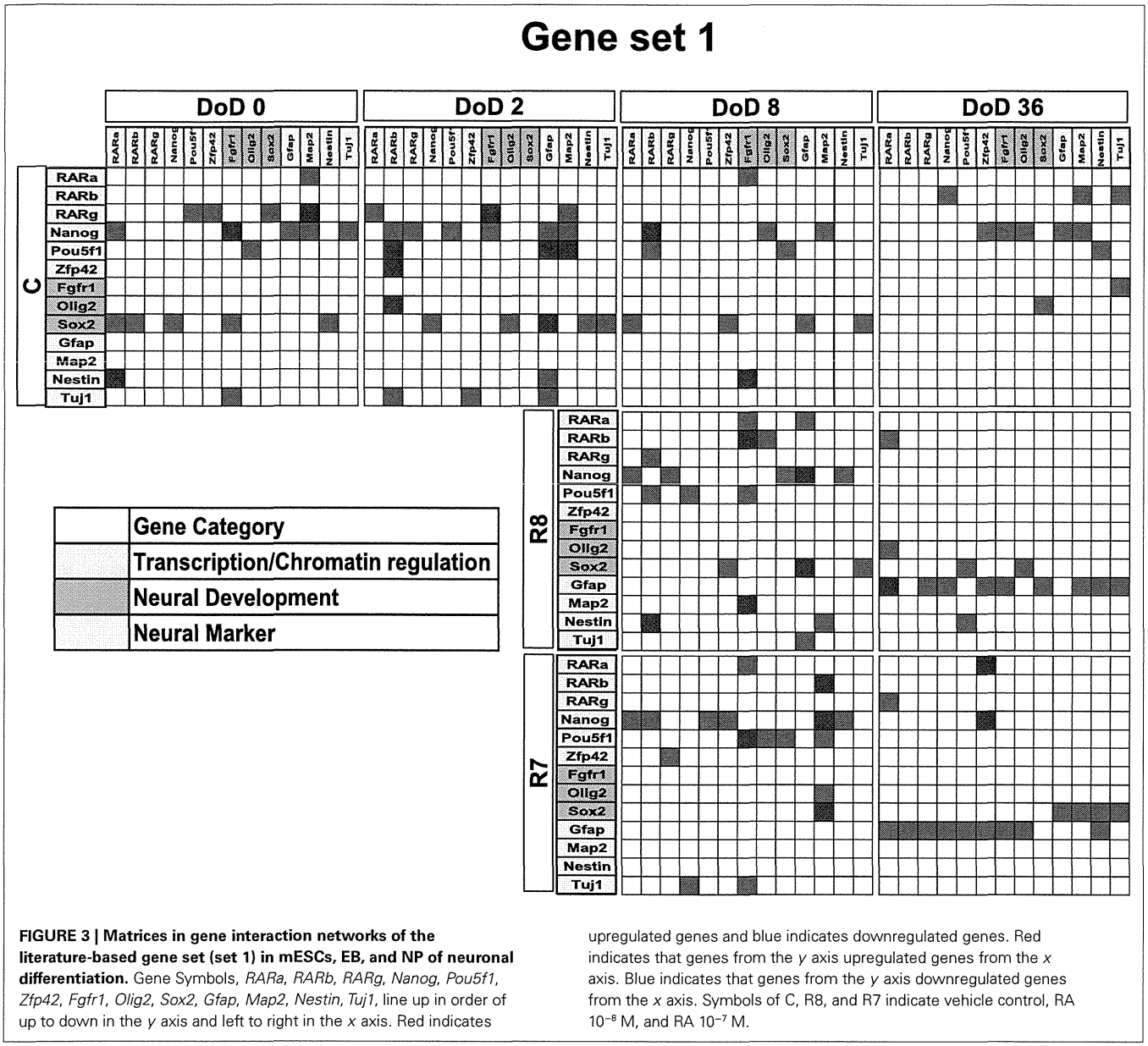

FIGURE 3 | Matrices in gene interaction networks of the literature-based gene set (set 1) in mESCs, EB, and NP of neuronal differentiation. Gene Symbols, *RARa, RARb, RARg, Nanog, Pou5f1, Zfp42, Fgfr1, Olig2, Sox2, Gfap, Map2, Nestin, Tuj1*, line up in order of up to down in the *y* axis and left to right in the *x* axis. Red indicates upregulated genes and blue indicates downregulated genes. Red indicates that genes from the *y* axis upregulated genes from the *x* axis. Blue indicates that genes from the *y* axis downregulated genes from the *x* axis. Symbols of C, R8, and R7 indicate vehicle control, RA 10^{-8} M, and RA 10^{-7} M.

network analysis was effective to identify the functions of the well-known neural development regulators, such as *Gfap* and *SOX2* (**Figures 3–5**), in response to RA during the neural differentiation of mESCs and suggested its further application to predict developmental neurotoxicity of environmental chemicals. However, in the simulation analysis, one major problem is to select genetic markers related with a trait of interest. To perform accurate simulation, it is undesirable to select genes with similar expression patterns. Similar variables could significantly affect the analysis results and potentially lead to biased results. Hence, the selection of genes with distinct expression patterns, which can represent each stage of mESC neural differentiation, seems to be important in the outcome of the GIN analysis. In this study, we selected gene sets for GIN analysis by the combined use of two classification methods, SOM and PCA. SOM is a powerful data mining method, whose algorithm is an unsupervised competitive learning neural network and it maps high-dimensional data into a simple low-dimensional display (Kohonen, 1990; Zhang et al., 2008). Therefore, SOM is able to classify the temporal expression data for each gene. After classification by SOM based on gene expression patterns, the representative genes were further selected from each class by PCA. PCA is a standard technique of pattern recognition and has been widely used as a tool in exploratory data analysis and for making predictive models in many biological systems (Aiba et al., 2006; van Dartel et al., 2010; Qin et al., 2011). In this study, the genes selected by SOM and PCA were shown to have adequate simulation parameters to evaluate the effects of RA on the neural differentiation of mESCs.

Finally, our prediction model, employing Bayesian network analysis, showed that it is possible to capture genetic correlations

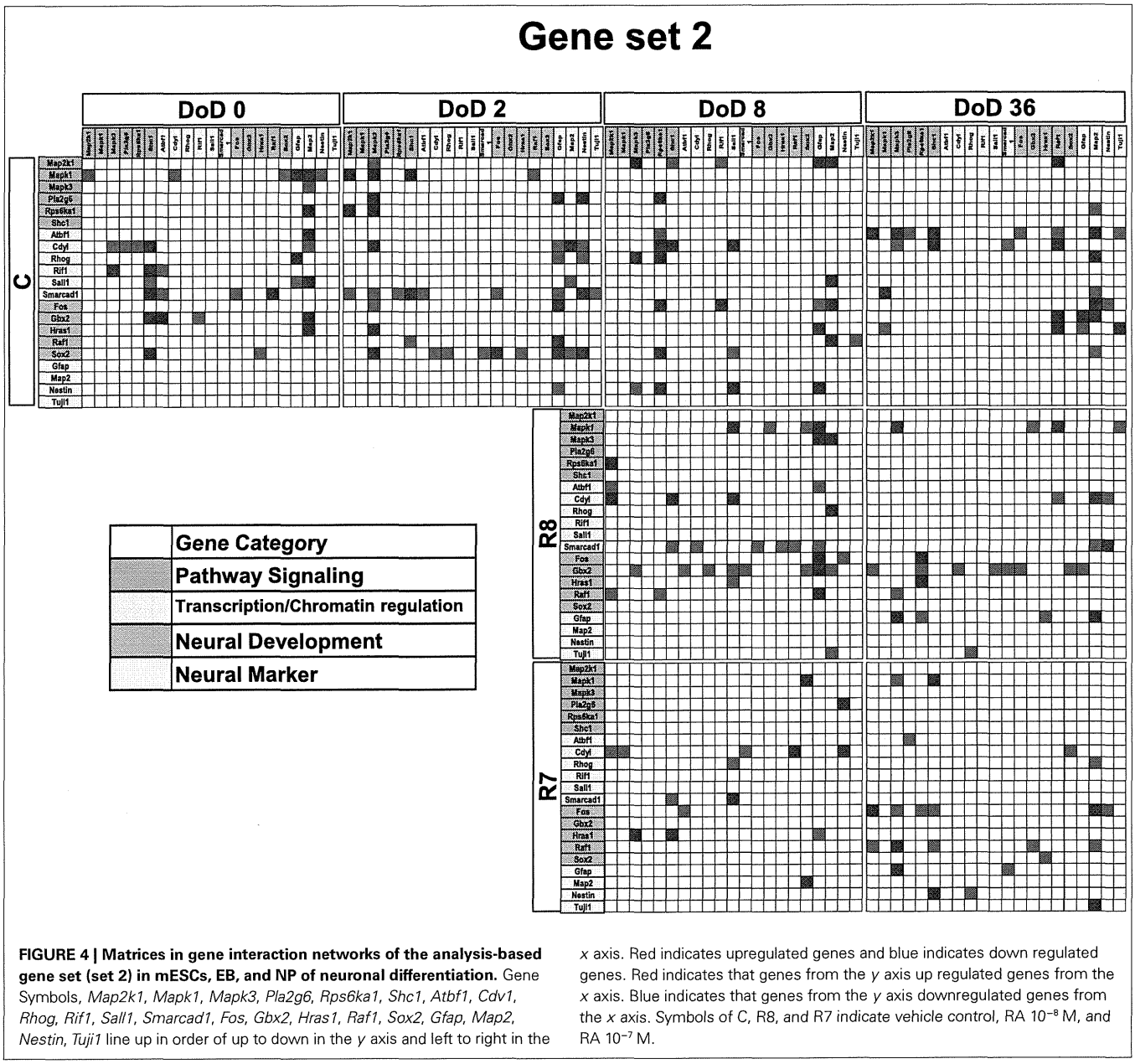

FIGURE 4 | Matrices in gene interaction networks of the analysis-based gene set (set 2) in mESCs, EB, and NP of neuronal differentiation. Gene Symbols, *Map2k1*, *Mapk1*, *Mapk3*, *Pla2g6*, *Rps6ka1*, *Shc1*, *Atbf1*, *Cdv1*, *Rhog*, *Rif1*, *Sall1*, *Smarcad1*, *Fos*, *Gbx2*, *Hras1*, *Raf1*, *Sox2*, *Gfap*, *Map2*, *Nestin*, *Tuji1* line up in order of up to down in the *y* axis and left to right in the *x* axis. Red indicates upregulated genes and blue indicates down regulated genes. Red indicates that genes from the *y* axis up regulated genes from the *x* axis. Blue indicates that genes from the *y* axis downregulated genes from the *x* axis. Symbols of C, R8, and R7 indicate vehicle control, RA 10^{-8} M, and RA 10^{-7} M.

between genes and to identify slight variations for different conditions. We performed the same prediction model for three gene sets of different genetic constitution. Our study indicated that the GIN was able to capture features of each developmental stage during the neural differentiation of mESCs. RA treatment could change the network structure in a dose-dependent manner. In addition, among the three gene sets, set 3 was the best according to the morphological results. We found that the *Gfap* gene was linked with other genes in the RA 10^{-7} M matrix in the GIN analysis, while the number of *Gfap*-positive cells was markedly increased by RA 10^{-7} M treatment on DoD 36 in the morphological analysis. This suggested that the approach used in this study, of the independent selection of gene sets using SOM or PCA, was efficient. This Bayesian model might also be useful to investigate the developmental toxicity of environmental chemicals other than RA.

In summary, to find the optimized GIN that integrated chemical effects, we created three different gene sets and then performed GIN analysis using Bayesian network algorithms to capture the stage-specific gene expression signatures in response to RA treatment during the neural differentiation of mESCs. "*Toxicity Testing in the Twenty First Century – A vision and a strategy*" issued by the US Nuclear Regulatory Commission indicated that the most important issue for toxicity testing is how to connect the extensive body of toxicity information to high-throughput screening to perform chemical risk assessment (Thomas et al., 2007; Davis et al., 2008; Ellinger-Ziegelbauer et al., 2009; Hubal, 2009). Here, we described a novel approach to identify stage-specific

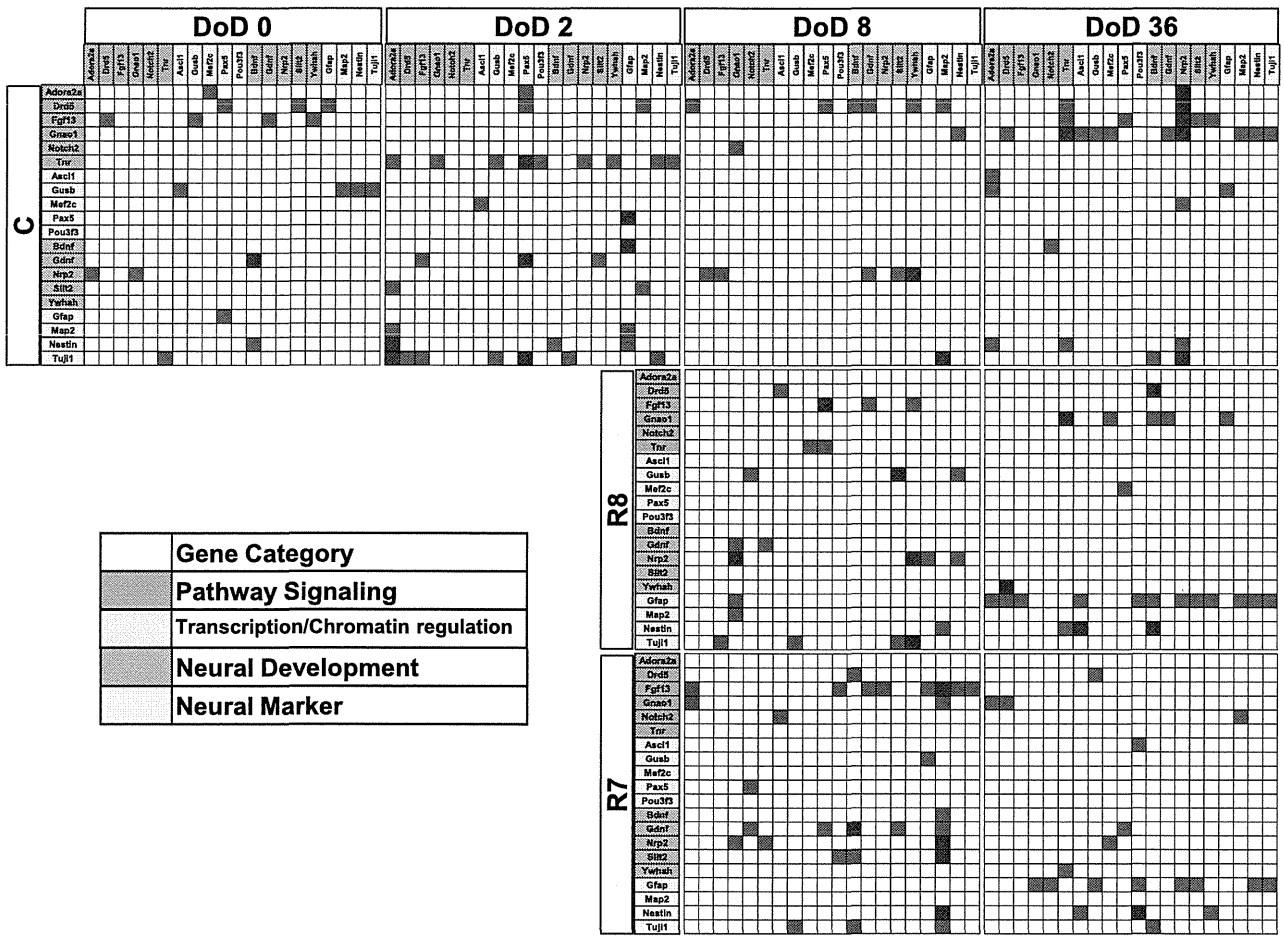

FIGURE 5 | Matrices in gene interaction networks of the enrichment gene set (set 3) in mESCs, EB, and NP of neuronal differentiation. Gene Symbols, *Adora2a, Drd5, Fgf13, Gnao1, Notch2, Tnr, Ascl1, Gusb, Mef2c, Pax5, Pou3f3, Bdnf, Gdnf, Nrp2, Slit2, Ywhah, Gfap, Map2, Nestin, Tujl1* line up in order of up to down in the *y* axis and left to right in the *x* axis. Red indicates up regulated genes and blue indicates down regulated genes. Red indicates that genes from the *y* axis up regulated genes from the *x* axis. Blue indicates that genes from the *y* axis down regulated genes from the *x* axis. Symbols of C, R8, and R7 indicate vehicle control, RA 10^{-8} M, and RA 10^{-7} M.

gene expression in embryonic development and suggested its application to evaluate the neural developmental toxicity of environmental chemicals in future studies.

ACKNOWLEDGMENTS

This study was supported, in part, by the Environmental Technology Development Fund (to Hideko Sone) from the Ministry of the Environment and by a Grant-in-Aid for Scientific Research from the Ministry of Health, Labour and Welfare, Japan (to Seiichiroh Ohsako). The authors gratefully acknowledge the technical support of Ms Noriko Oshima (GE Healthcare Corporation, Japan) for analysis using the IN Cell Analyzer 1000.

SUPPLEMENTARY MATERIAL

The Supplementary Material for this article can be found online at: http://www.frontiersin.org/Toxicogenomics_/10.3389/fgene.2012.00141/abstract

Table S1 | Input data of gene expression values for set 1. Values are normalized expression values in beads of each gene with approximate 30 replicates.

Table S2 | Input data of gene expression values for set 2. Values are normalized expression values in beads of each gene with approximate 30 replicates.

Table S3 | Input data of gene expression values for set 3. Values are normalized expression values in beads of each gene with approximate 30 replicates.

Table S4 | Output results of the Bayesian network analysis with gene expression values for set 1. Values are posterior probabilities.

Table S5 | Output results of the Bayesian network analysis with gene expression values for set 2. Values are posterior probabilities.

Table S6 | Output results of the Bayesian network analysis with gene expression values for set 3. Values are posterior probabilities.

REFERENCES

Ahn, S. M., Byun, K., Kim, D., Lee, K., Yoo, J. S., Kim, S. U., Jho, E. H., Simpson, R. J., and Lee, B. (2008). Olig2-induced neural stem cell differentiation involves downregulation of Wnt signaling and induction of Dickkopf-1 expression. *PLoS ONE* 3, e3917. doi:10.1371/journal.pone.0003917

Aiba, K., Sharov, A. A., Carter, M. G., Foroni, C., Vescovi, A. L., and Ko, M. S. (2006). Defining a developmental path to neural fate by global expression profiling of mouse embryonic stem cells and adult neural stem/progenitor cells. *Stem Cells* 24, 889–895.

Akamatsu, W., Deveale, B., Okano, H., Cooney, A. J., and van der Kooy, D. (2009). Suppression of Oct-4 by germ cell nuclear factor restricts pluripotency and promotes neural stem cell development in the early neural lineage. *J. Neurosci.* 29, 2113–2124.

Asano, H., Aonuma, M., Sanosaka, T., Kohyama, J., Namihira, M., and Nakashima, K. (2009). Astrocyte differentiation of neural precursor cells is enhanced by retinoic acid through a change in epigenetic modification. *Stem Cells* 27, 2744–2752.

Catena, R., Tiveron, C., Ronchi, A., Porta, S., Ferri, A., Tatangelo, L., Cavallaro, M., Favaro, R., Ottolenghi, S., Reinbold, R., Schöler, H., and Nicolis, S. K. (2004). Conserved POU binding DNA sites in the Sox2 upstream enhancer regulate gene expression in embryonic and neural stem cells. *J. Biol. Chem.* 279, 41846–41857.

Cosgaya, J. M., Garcia-Villalba, P., Perona, R., and Aranda, A. (1996). Comparison of the effects of retinoic acid and nerve growth factor on PC12 cell proliferation, differentiation, and gene expression. *J. Neurochem.* 66, 89–98.

Davis, A. P., Murphy, C. G., Rosenstein, M. C., Wiegers, T. C., and Mattingly, C. J. (2008). The Comparative Toxicogenomics Database facilitates identification and understanding of chemical-gene-disease associations: arsenic as a case study. *BMC Med. Genomics* 1, 48. doi:10.1186/1755-8794-1-48

Ellinger-Ziegelbauer, H., Fostel, J. M., Aruga, C., Bauer, D., Boitier, E., Deng, S. B., Dickinson, D., Le Fevre, A. C., Fornace, A. J., Grenet, O., Gu, Y. Z., Hoflack, J. C., Shiiyama, M., Smith, R., Snyder, R. D., Spire, C., Tanaka, G., and Aubrechtk, J. (2009). Characterization and interlaboratory comparison of a gene expression signature for differentiating genotoxic mechanisms. *Toxicol. Sci.* 110, 341–352.

Engberg, N., Kahn, M., Petersen, D. R., Hansson, M., and Serup, P. (2010). Retinoic acid synthesis promotes development of neural progenitors from mouse embryonic stem cells by suppressing endogenous, Wnt-dependent nodal signaling. *Stem Cells* 28, 1498–1509.

Graham, V., Khudyakov, J., Ellis, P., and Pevny, L. (2003). SOX2 functions to maintain neural progenitor identity. *Neuron* 39, 749–765.

Harnisha, D. C., Baruad, A. B., Sopranob, K. J., and Soprano, D. R. (1990). Induction of β-retinoic acid receptor mRNA by teratogenic doses of retinoids in murine fetuses. *Differentiation* 45, 103–108.

Hubal, E. A. C. (2009). Biologically relevant exposure science for 21st century toxicity testing. *Toxicol. Sci.* 111, 226–232.

Jin, Z., Liu, L., Bian, W., Chen, Y., Xu, G., Cheng, L., and Jing, N. (2009). Different transcription factors regulate nestin gene expression during P19 cell neural differentiation and central nervous system development. *J. Biol. Chem.* 284, 8160–8173.

Jukkola, T., Lahti, L., Naserke, T., Wurst, W., and Partanen, J. (2006). FGF regulated gene-expression and neuronal differentiation in the developing midbrain-hindbrain region. *Dev. Biol.* 297, 141–157.

Kawasaki, H., Mizuseki, K., Nishikawa, S., Kaneko, S., Kuwana, Y., Nakanishi, S., Nishikawa, S. I., and Sasai, Y. (2000). Induction of midbrain dopaminergic neurons from ES cells by stromal cell-derived inducing activity. *Neuron* 28, 31–40.

Kohonen, T. (1990). The self-organizing map. *Proc. IEEE* 78, 1464–1480.

Lamoury, F. M. J., Croitoru-Lamoury, J., and Brew, B. J. (2006). Undifferentiated mouse mesenchymal stem cells spontaneously express neural and stem cell markers Oct-4 and Rex-1. *Cytotherapy* 8, 228–242.

Lee, D. C., Hsu, Y. C., Chung, Y.-F., Hsiao, C. Y., Chen, S. L., Chen, M.-S., Lin, H. K., and Chiu, I.-M. (2009). Isolation of neural stem/progenitor cells by using EGF/FGF1 and FGF1B promoter-driven green fluorescence from embryonic and adult mouse brains. *Mol. Cell. Neurosci.* 41, 348–363.

Ligon, K. L., Kesari, S., Kitada, M., Sun, T., Arnett, H. A., Alberta, J. A., Anderson, D. J., Stiles, C. D., and Rowitch, D. H. (2006). Development of NG2 neural progenitor cells requires Olig gene function. *Proc. Natl. Acad. Sci. U.S.A.* 103, 7853–7858.

Loh, Y. H., Wu, Q., Chew, J. L., Vega, V. B., Zhang, W., Chen, X., Bourque, G., George, J., Leong, B., Liu, J., Wong, K. Y., Sung, K. W., Lee, C. W., Zhao, X. D., Chiu, K. P., Lipovich, L., Kuznetsov, V. A., Robson, P., Stanton, L. W., Wei, C. L., Ruan, Y., Lim, B., and Ng, H. H. (2006). The Oct-4 and Nanog transcription network regulates pluripotency in mouse embryonic stem cells. *Nat. Genet.* 38, 431–440.

Maden, M., Sonneveld, E., van der Saag, P. T., and Gale, E. (1998). The distribution of endogenous retinoic acid in the chick embryo: implications for developmental mechanisms. *Development* 125, 4133–4144.

Mic, F. A., Molotkov, A., Benbrook, D. M., and Duester, G. (2003). Retinoid activation of retinoic acid receptor but not retinoid X receptor is sufficient to rescue lethal defect in retinoic acid synthesis. *Proc. Natl. Acad. Sci. U.S.A.* 100, 7135–7140.

Mitsui, K., Tokuzawa, Y., Itoh, H., Segawa, K., Murakami, M., Takahashi, K., Maruyama, M., Maeda, M., and Yamanaka, S. (2003). The homeoprotein Nanog is required for maintenance of pluripotency in mouse epiblast and ES Cells. *Cell* 113, 631–642.

Miyazaki, K., Narita, N., and Narita, M. (2005). Maternal administration of thalidomide or valproic acid causes abnormal serotonergic neurons in the offspring: implication for pathogenesis of autism. *Int. J. Dev. Neurosci.* 23, 287–297.

Nagano, R., Akanuma, H., Qin, X. Y., Imanishi, S., Toyoshiba, H., Yoshinaga, J., Ohsako, S., and Sone, H. (2012). Multi-parametric profiling network based on gene expression and phenotype data: a novel approach to developmental neurotoxicity testing. *Int. J. Mol. Sci.* 13, 187–207.

Nishimura, F., Yoshikawa, M., Kanda, S., Nonaka, M., Yokota, H., Shiroi, A., Nakase, H., Hirabayashi, H., Ouji, Y., Birumachi, J., Ishizaka, S., and Sakaki, T. (2003). Potential use of embryonic stem cells for the treatment of mouse parkinsonian models: improved behavior by transplantation of in vitro differentiated dopaminergic neurons from embryonic stem cells. *Stem Cells* 21, 171–180.

Okada, Y., Shimazaki, T., Sobue, G., and Okano, H. (2004). Retinoic-acid-concentration-dependent acquisition of neural cell identity during in vitro differentiation of mouse embryonic stem cells. *Dev. Biol.* 275, 124–142.

Okazawa, H., Okamoto, K., Ishino, F., Ishinokaneko, T., Takeda, S., Toyoda, Y., Muramatsu, M., and Hamada, H. (1991). The Oct3 gene, a gene for an embryonic transcription factor, is controlled by a retinoic acid repressible enhancer. *EMBO J.* 10, 2997–3005.

Qin, X. Y., Wei, F., Yoshinaga, J., Yonemoto, J., Tanokura, M., and Sone, H. (2011). siRNA-mediated knockdown of aryl hydrocarbon receptor nuclear translocator 2 affects hypoxia-inducible factor-1 regulatory signaling and metabolism in human breast cancer cells. *FEBS Lett.* 585, 3310–3315.

Schuldiner, M., Eiges, R., Eden, A., Yanuka, O., Itskovitz-Eldor, J., Goldstein, R. S., and Benvenisty, N. (2001). Induced neuronal differentiation of human embryonic stem cells. *Brain Res.* 913, 201–205.

Scotland, K. B., Chen, S., Sylvester, R., and Gudas, L. J. (2009). Analysis of Rex1 (zfp42) function in embryonic stem cell differentiation. *Dev. Dyn.* 238, 1863–1877.

Seiler, A. E., Buesen, R., Visan, A., and Spielmann, H. (2006). Use of murine embryonic stem cells in embryotoxicity assays: the embryonic stem cell test. *Methods Mol. Biol.* 329, 371–395.

Shi, W., Wang, H., Pan, G., Geng, Y., Guo, Y., and Pei, D. (2006). Regulation of the pluripotency marker Rex-1 by Nanog and Sox2. *J. Biol. Chem.* 281, 23319–23325.

Shiotsugu, J., Katsuyama, Y., Arima, K., Baxter, A., Koide, T., Song, J., Chandraratna, R. A., and Blumberg, B. (2004). Multiple points of interaction between retinoic acid and FGF signaling during embryonic axis formation. *Development* 131, 2653–2667.

So, P. L., Yip, P. K., Bunting, S., Wong, L. F., Mazarakis, N. D., Hall, S., Mcmahon, S., Maden, M., and Corcoran, J. P. (2006). Interactions between retinoic acid, nerve growth factor and sonic hedgehog signalling pathways in neurite outgrowth. *Dev. Biol.* 298, 167–175.

Tanaka, S., Kamachi, Y., Tanouchi, A., Hamada, H., Jing, N., and Kondoh, H. (2004). Interplay of SOX and POU factors in regulation of the Nestin gene in neural primordial cells. *Mol. Cell. Biol.* 24, 8834–8846.

Thomas, R. S., Allen, B. C., Nong, A., Yang, L., Bermudez, E., Clewell,

H. J., and Andersen, M. E. (2007). A method to integrate benchmark dose estimates with genomic data to assess the functional effects of chemical exposure. *Toxicol. Sci.* 98, 240–248.

Tomioka, M., Nishimoto, M., Miyagi, S., Katayanagi, T., Fukui, N., Niwa, H., Muramatsu, M., and Okuda, A. (2002). Identification of Sox-2 regulatory region which is under the control of Oct-3/4-Sox-2 complex. *Nucleic Acids Res.* 30, 3202–3213.

Toyoshiba, H., Sone, H., Yamanaka, T., Parham, F. M., Irwin, R. D., Boorman, G. A., and Portier, C. J. (2006). Gene interaction network analysis suggests differences between high and low doses of acetaminophen. *Toxicol. Appl. Pharmacol.* 215, 306–316.

Toyoshiba, H., Yamanaka, T., Sone, H., Parham, F. M., Walker, N. J., Martinez, J., and Portier, C. J. (2004). Gene interaction network suggests dioxin induces a significant linkage between aryl hydrocarbon receptor and retinoic acid receptor beta. *Environ. Health Perspect.* 112, 1217–1224.

van Dartel, D. A. M., Pennings, J. L. A., Van Schooten, F. J., and Piersma, A. H. (2010). Transcriptomics-based identification of developmental toxicants through their interference with cardiomyocyte differentiation of embryonic stem cells. *Toxicol. Appl. Pharmacol.* 243, 420–428.

Veiga Quemelo, P. R., Lourenco, C. M., and Peres, L. C. (2007). Teratogenic effect of retinoic acid in swiss mice. *Acta Cir. Bras.* 22, 451–456.

Wilson, L., and Maden, M. (2005). The mechanisms of dorsoventral patterning in the vertebrate neural tube. *Dev. Biol.* 282, 1–13.

Yamanaka, T., Toyoshiba, H., Sone, H., Parham, F. M., and Portier, C. J. (2004). The TAO-Gen algorithm for identifying gene interaction networks with application to SOS repair in *E. coli*. *Environ. Health Perspect.* 112, 1614–1621.

Yang, H., Xia, Y., Lu, S. Q., Soong, T. W., and Feng, Z. W. (2008). Basic fibroblast growth factor-induced neuronal differentiation of mouse bone marrow stromal cells requires FGFR-1, MAPK/ERK, and transcription factor AP-1. *J. Biol. Chem.* 283, 5287–5295.

Zhang, Y. J., Xuan, J. H., de los Reyes, B. G., Clarke, R., and Ressom, H. W. (2008). Network motif-based identification of transcription factor-target gene relationships by integrating multi-source biological data. *BMC Bioinformatics* 9, 203. doi:10.1186/1471-2105-9-203

Conflict of Interest Statement: The authors declare that the research was conducted in the absence of any commercial or financial relationships that could be construed as a potential conflict of interest.

Received: 27 March 2012; accepted: 12 July 2012; published online: 07 August 2012.

Citation: Akanuma H, Qin X-Y, Nagano R, Win-Shwe T-T, Imanishi S, Zaha H, Yoshinaga J, Fukuda T, Ohsako S and Sone H (2012) Identification of stage-specific gene expression signatures in response to retinoic acid during the neural differentiation of mouse embryonic stem cells. Front. Gene. 3:141. doi: 10.3389/fgene.2012.00141

This article was submitted to Frontiers in Toxicogenomics, a specialty of Frontiers in Genetics.

APPENDIX

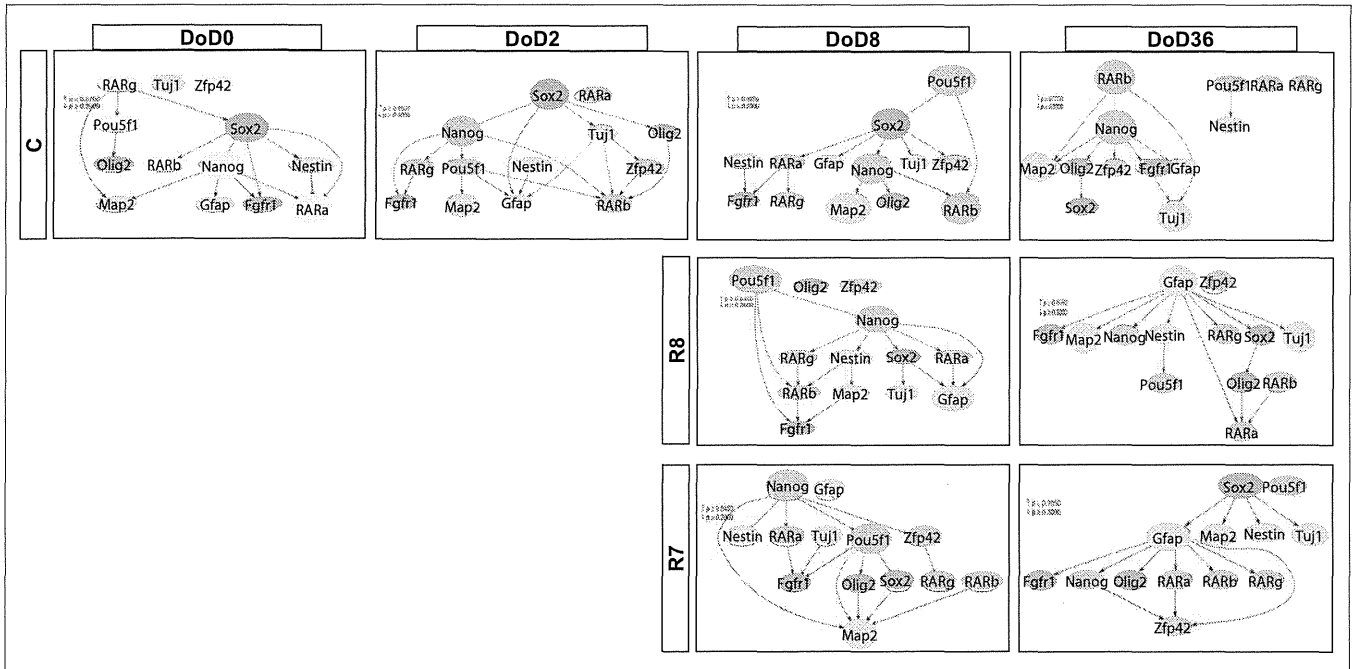

FIGURE A1 | Gene interaction networks of the literature-based gene set (set 1) in mESCs, EB, and NP of neuronal differentiation. The optimized network was generated at $p > 0.300$. Red indicates that parent genes up-regulate children genes. Blue indicates that parent genes down-regulate children genes.

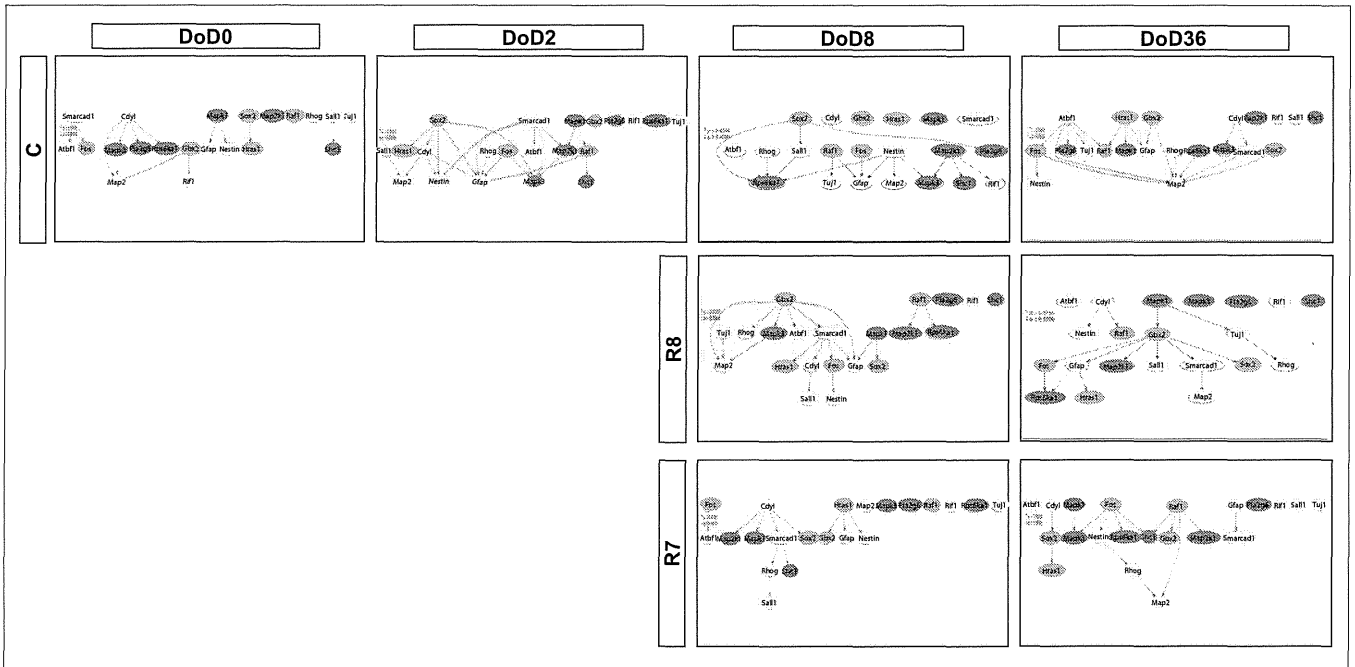

FIGURE A2 | Gene interaction networks of the analysis-based gene set (set 2) in mESCs, EB, and NP of neuronal differentiation. The optimized network was generated at $p > 0.300$. Red indicates that parent genes up-regulate children genes. Blue indicates that parent genes down-regulate children genes.

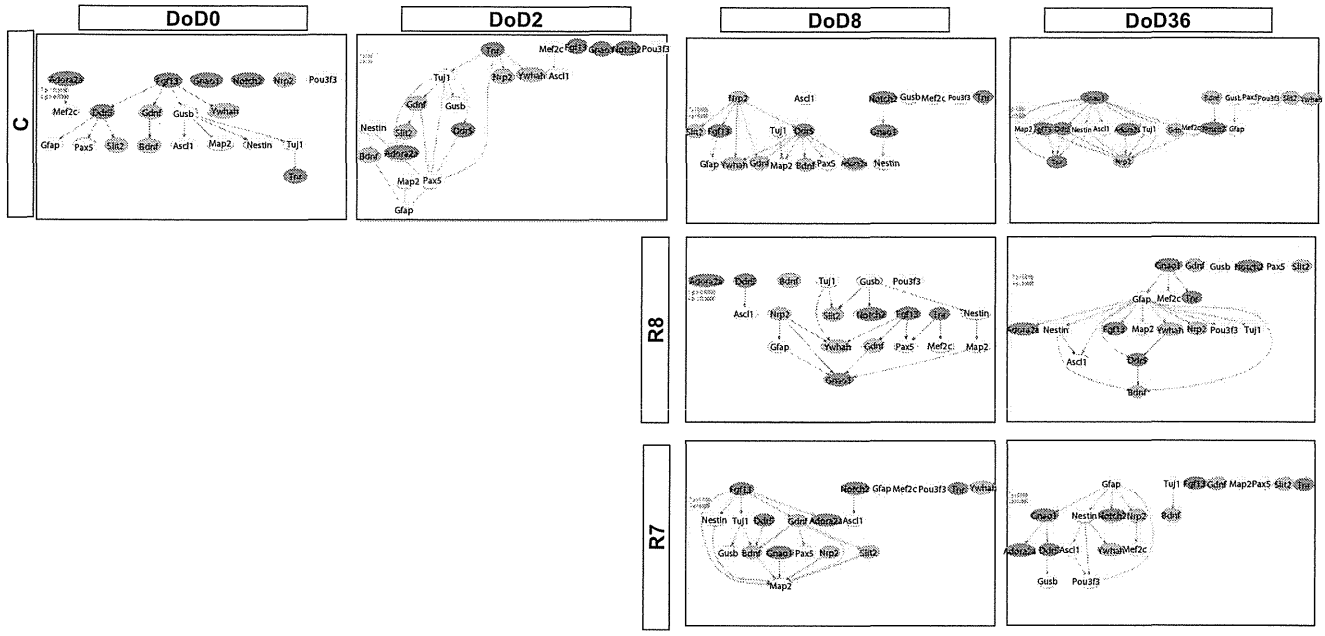

FIGURE A3 | Gene interaction networks of the enrichment gene set (set 3) in mESCs, EB, and NP of neuronal differentiation. The optimized network was generated at $p > 0.300$. Red indicates that parent genes up-regulate children genes. Blue indicates that parent genes down-regulate children genes.

Toxicology Letters 212 (2012) 1–10

Contents lists available at SciVerse ScienceDirect

Toxicology Letters

journal homepage: www.elsevier.com/locate/toxlet

Effects of methylmercury exposure on neuronal differentiation of mouse and human embryonic stem cells

Xiaoming He[a,1], Satoshi Imanishi[a,1], Hideko Sone[b,*], Reiko Nagano[b], Xian-Yang Qin[b,c], Jun Yoshinaga[c], Hiromi Akanuma[b], Junko Yamane[a], Wataru Fujibuchi[d], Seiichiroh Ohsako[a]

[a] Division of Environmental Health Sciences, Center for Disease Biology and Integrative Medicine, Graduate School of Medicine, The University of Tokyo, 7-3-1 Hongo, Bunkyo-ku, Tokyo 113-8654, Japan
[b] Research Center for Environmental Risk, National Institute for Environmental Studies, 16-2 Onogawa, Tsukuba, Ibaraki 305-8506, Japan
[c] Department of Environmental Studies, Graduate School of Frontier Science, The University of Tokyo, 5-1-5 Kashiwanoha, Kashiwa, Chiba 270-8563, Japan
[d] Computational Biology Research Center, Advanced Industrial Science and Technology (AIST), 2-4-7 Aomi, Koto-ku, Tokyo 135-0064, Japan

ARTICLE INFO

Article history:
Received 26 January 2012
Received in revised form 13 April 2012
Accepted 16 April 2012
Available online xxx

Keywords:
Methylmercury
Human
Embryonic stem cells
Neuronal development
Alternative method

ABSTRACT

The establishment of more efficient *in vitro* approaches has been widely acknowledged as a critical need for toxicity testing. In this study, we examined the effects of methylmercury (MeHg), which is a well-known developmental neurotoxicant, in two neuronal differentiation systems of mouse and human embryonic stem cells (mESCs and hESCs, respectively). Embryoid bodies were generated from gathering of mESCs and hESCs using a micro-device and seeded onto ornithine–laminin-coated plates to promote proliferation and neuronal differentiation. The cells were exposed to MeHg from the start of neuronal induction until the termination of cultures, and significant reductions of mESCs and hESCs were observed in the cell viability assays at 1,10,100 and 1000 nM, respectively. Although the mESC derivatives were more sensitive than the hESC derivatives to MeHg exposure in terms of cell viability, the morphological evaluation demonstrated that the neurite length and branch points of hESC derivatives were more susceptible to a low concentration of MeHg. Then, the mRNA levels of differentiation markers were examined using quantitative RT-PCR analysis and the interactions between MeHg exposure and gene expression levels were visualized using a network model based on a Bayesian algorithm. The Bayesian network analysis showed that a MeHg-node was located on the highest hierarchy in the hESC derivatives, but not in the mESC derivatives, suggesting that MeHg directly affect differentiation marker genes in hESCs. Taken together, effects of MeHg were observed in our neuronal differentiation systems of mESCs and hESCs using a combination of morphological and molecular markers. Our study provided possible, but limited, evidences that human ESC models might be more sensitive in particular endpoints in response to MeHg exposure than that in mouse ESC models. Further investigations that expand on the findings of the present paper may solve problems that occur when the outcomes from laboratory animals are extrapolated for human risk evaluation.

1. Introduction

Methylmercury (MeHg) has severely poisoned over tens of thousands of individuals in Japan and in Iraq, and exposure to small amounts of MeHg through the consumption of fish, shellfish, or sea mammals continues to be an issue (Airaksinen et al., 2010; Kuntz et al., 2010). Nearly all humans worldwide have trace amounts of MeHg in their tissues, which suggest widespread presence of MeHg in the environment (Grandjean et al., 2010). In addition, MeHg can cause neurotoxicity during pregnancy, even in the absence of maternal toxicity (*i.e.*, the human infants suffered a so-called congenital Minamata disease and exhibit severe developmental disabilities, such as cerebral palsy, mental retardation, convulsive seizures and muscle rigidity) (Davidson et al., 2004; Harada et al., 1999). Despite the simultaneous exposure of a mother and an infant during pregnancy, serious symptoms have not been observed in mothers, which suggests that the fetal brain is highly sensitive to MeHg (Davidson et al., 2004; Harada et al., 1999); however, no information is available on dose–response relationships in

Abbreviations: MeHg, methylmercury; DMSO, dimethyl sulfoxide; MSA, microsphere-array; EB, embryoid body; hESC, human embryonic stem cell; mESC, mouse embryonic stem cell; EST, embryonic stem cell test; hNPC, human neuronal precursor cells; ECVAM, European Center for the Validation of Alternative Methods; ICA, IN Cell Analyzer.

* Corresponding author. Tel.: +81 29 850 2464; fax: +81 29 850 2546.
E-mail address: hsone@nies.go.jp (H. Sone).
[1] These authors contributed equally.

0378-4274/$ – see front matter © 2012 Elsevier Ireland Ltd. All rights reserved.
http://dx.doi.org/10.1016/j.toxlet.2012.04.011

these children. Laboratory mice and rats do not exhibit the typical symptoms of congenital Minamata disease following similar MeHg exposures during pregnancy despite frequent fetal and infant deaths following exposure to a relatively low dose of MeHg *in utero* (Choi, 1989; Hu et al., 2010; Satoh and Suzuki, 1983; Weiss et al., 2005). These findings suggest that the susceptibility of developing neuronal cells in the human fetus to MeHg is distinct and more severe from the susceptibility of laboratory animals.

Embryonic stem cells (ESCs) can differentiate *in vitro* into cells of all three embryonic germ layers, which reflect to some extent, the *in vivo* development of the embryo. This concept has provided the scientific rationale for emerging research on the use of ESCs to establish tests for toxicity to the early embryo. An embryonic stem cell test (EST) using a cardiac differentiation system from mouse ESCs (mESCs) is advocated by the European Center for the Validation of Alternative Methods (ECVAM) as one of alternative methods for *in vivo* embryo toxicity (Genschow et al., 2004). Researchers believe that the development of an EST that is based on human ESCs (hESCs) will provide an ideal tool for the assessment of human embryo toxicity because such a system will improve the prediction of human hazards while reducing the requirement for laboratory animals. In addition, a hESC-based EST would limit the need to consider interspecies differences (Reubinoff et al., 2000; Thomson et al., 1998). Many researchers are currently attempting to develop a human EST to evaluate the effects of chemicals on cardiac and neuronal differentiation (Murabe et al., 2007; Stummann and Bremer, 2008; Stummann et al., 2009; Wada et al., 2009).

The toxicity of MeHg has been examined in several ESCs-derived neural developmental models and the endpoints generally used included cell survival, cell morphology, transcript changes, and so on (Baek et al., 2011; Stummann et al., 2009; Tamm et al., 2006; Theunissen et al., 2011). In this study, we described two neuronal differentiation systems of mESCs and hESCs and examined the effects of MeHg using a combination of morphological and molecular markers. The advantages of our study might include: (1) the use of mouse *vs.* human ESCs provided a potential approach to explore/understand species differences; (2) the incorporation of the morphological endpoint in addition to the usual mRNA expression could provide detailed mechanistic insight to improve the EST for the assessments of developmental neurotoxicants.

2. Materials and methods

2.1. Culture and neuronal differentiation of ESCs

The mESC line, B6G-2 (XY genotype), was provided from RIKEN BioResource Center and maintained as described (Shimizukawa et al., 2005). The hESC line, KhES-3 (XY genotype), was provided by Dr. Hirofumi Suemori, Research Center of Stem Cells, Institute for Frontier Medical Science, Kyoto University (Suemori et al., 2006). All experiments using hESCs were approved by the ethics committees of the National Institute for Environmental Studies and the University of Tokyo in accordance with to the guideline of the Japanese Ministry of Education, Culture, Sports, Science, and Technology. The procedures for the maintenance of mESCs and hESCs were performed as described previously (Shimizukawa et al., 2005; Suemori et al., 2006). Both mESCs and hESCs were allowed to form embryoid bodies (EBs) in the micro-device of microsphere-array (MSA; 1020 holes, φ 300 μm/hole, STEM Biomethods, Japan). The EBs were seeded onto ornithine–laminin (O/L)-coated 24-well plates to promote proliferation and neuronal differentiation with the sequential exchange of authentic appropriate neuronal differentiation media. The schedules for the neuronal differentiation of mESCs and hESCs are summarized in Figs. 1A and 2B, respectively. Exposure to MeHg (0.001% DMSO) began on Day 12 or Day 27 and continued until Day 23 or Day 50 for the mESC and hESC derivatives, respectively. The medium containing MeHg was refreshed every 3 days (see details in Supplemental Material, Methods).

2.2. MTT assay

Cytotoxicity was measured in terms of reduced mitochondrial activity using the MTT-Assay Kit. EB-derived cells were plated onto O/L-coated 96-well plates, and a 10-μl of aliquot of 3-(4,5-dimethyl-2-thiazolyl)-2,5-diphenyltetrazolium bromide was added to the cells at each time point and incubated for 4 h. After incubation, 100-μl of isopropyl alcohol was added. Following additional 24-h incubation, the optical density was measured at 570 nm. Standard curves were prepared for each cell type by counting cells derived from mESCs and hESCs that were cultured in medium without MeHg or DMSO.

2.3. Immunocytochemistry

Immunostaining of MAP2 was performed on Day 23 for mESCs (mESC-Day 23) and Day 50 for hESCs (hESC-Day 50). After fixation for 10 min with 4% paraformaldehyde, the cells were permeabilized in 0.1% Triton X-100 in PBS. The cells were incubated with 1% BSA, which was followed by overnight incubation with primary antibody specific for MAP2 (1:200). After PBS washing, the cells were incubated at room temperature for 1 h with Alexa 568-labeled secondary antibodies (1:1000). Nuclei were stained using 2 μg/ml of Hoechst 33342 for 15 min.

2.4. Morphological measurement by IN Cell Analyzer

Microphotographs were periodically obtained using Olympus IX70 22FL/PH inverted microscope (Olympus Optical, Japan). The morphological analysis was performed using an automatic multichannel imaging analyzer (IN Cell Analyzer 1000 (ICA), GE Healthcare UK Ltd., Buckinghamshire, UK). The microphotographs of 57 fields (0.60 mm^2) per well of 24 well plate (*i.e.*, 1368 fields per exposure group) were taken automatically. The fields in a well were created without overlap. The fluorescent signal detected by the 535-nm laser line combined with a HQ620 60 M emission filter was considered to be the MAP2-positive signal of neurons. The fluorescent signal detected using the 360-nm laser line combined with a HQ460 40 M emission filter was considered to indicate the Hoechst33342 positive nuclei. Fluorescence emission was separately recorded in the blue and red channels, and a flat field correction was applied for inhomogeneous illumination of the scanned area for each of the two channels.

A typical merged image of hESC-derivatives is shown in Fig. S1A. Hoechst-positive nuclei were recognized using IN Cell Developer Software (GE Healthcare UK Ltd.) and replaced by yellow dots to accurately count the nuclei number (Fig. S1B). MAP2-positive signals were also recognized by this software with a threshold appropriate for tracing the MAP2-postive neurites. The replaced pink images are shown in Fig. S1C. MAP2-positive signals surrounding nuclei were regarded as the cell bodies of differentiated neural cells. The number of nuclei within the cell body was considered to be the number of MAP2-positive neurons in each field. The areas considered to be cell bodies were subtracted from the MAP2-postive images to generate the image of the neurites as shown in Fig. S1D. Then the software automatically replaces the MAP2-positive neurite images with branching morphologies, which indicated neurite-length as green center lines and branching points as blue circles (Figs. S1D, S1E, and S1F). As shown in Supplemental Fig. S1E, the cell bodies were successfully distinguished from the neurites. The total length of the MAP2-positive projection was automatically measured on its midline (Fig. S1F). The values for neurite length/cell were calculated by dividing the total MAP2-positive neurite length within a field by the number of MAP2-positive neurons. The branching points of MAP2-positive projections were automatically counted as the total number of branching points of the MAP2-positive projections (Fig. S1F). The values for branching points/cell were calculated by dividing the total MAP2-positive neurite branching points within a field by the number of MAP2-positive neurons. The average of the neurite length/cell or branching points/cell of all fields in one well of the 24-well plate were indicated as the value of one experiment. Images of mESC-derived neuronal cells were analyzed in the same manner.

To evaluate the accuracy of ICA measurements, the total neurite lengths of 5 randomly selected fields were manually measured using ImageJ (IJ) software (NIH). The correlations between data from IN Cell Developer Software and from IJ are shown in Fig. S2. Although the values obtained by ICA tended to be higher (approximately 1.73-fold for neurite length and 4.42-fold for branching points), the two values obtained by ICA and IJ were well correlated, which demonstrated the accuracy of the ICA measurement.

2.5. Quantitative RT-PCR

Total RNA from the mESC or hESC derivatives was harvested with an RNeasy mini kit. Gene expression of neuronal differentiation markers (Table 1) in the mESC and hESC derivatives were investigated by semi-quantitative RT-PCR or quantitative RT-PCR (see primer information in Supplemental Material, Table S1) using a high-throughput real-time thermal cycler (Light Cycler 480 system, Roche, Basel, Switzerland). The quantitative data were obtained by calculating the absolute copy number as previously described (Sakata et al., 2007).

2.6. Network model analysis

The linkages between MeHg and differentiation marker gene indices were visualized using a network model that was based on a Bayesian algorithm modified from an algorithm defined in a previous study (Toyoshiba et al., 2004). In brief, the network was quantified to calculate the posterior probability distribution for the strength of the linkages on the basis of the gene expression datasets (see Supplemental Material, Table S2 and Table S3). A network was used to evaluate

the ability of the algorithm to have a higher posterior probability (p-value) at the correct linkage in the network (see the detail described in Supplemental Material, Methods).

2.7. Statistical analysis

Statistical analyses were performed with StatView for Windows, version 5.0 (SAS Institute, Cary, NC). All data were expressed relative to the means of the control groups. All results are represented as mean ± SE. A two-way analysis of variance (ANOVA) was used for the MTT assay to compare the effect of each dose with the DMSO control groups. Other data were analyzed by one-way ANOVA followed by Fisher's PLSD post hoc test. p-Values less than 0.05 were considered to be statistically significant.

Table 1
Selection of neuronal differentiation markers in this study.

Gene	Function	Reference
NODAL	Mesoendoderm formation	Tada et al. (2005)
PAX6	Cerebral cortex formation	Caric et al. (1997), Duparc et al. (2006)
EMX2	Cerebral cortex formation	Galli et al. (2002), Mallamaci et al. (2000)
Hoxb4	Paraximal mesoderm formation	Brend et al. (2003)

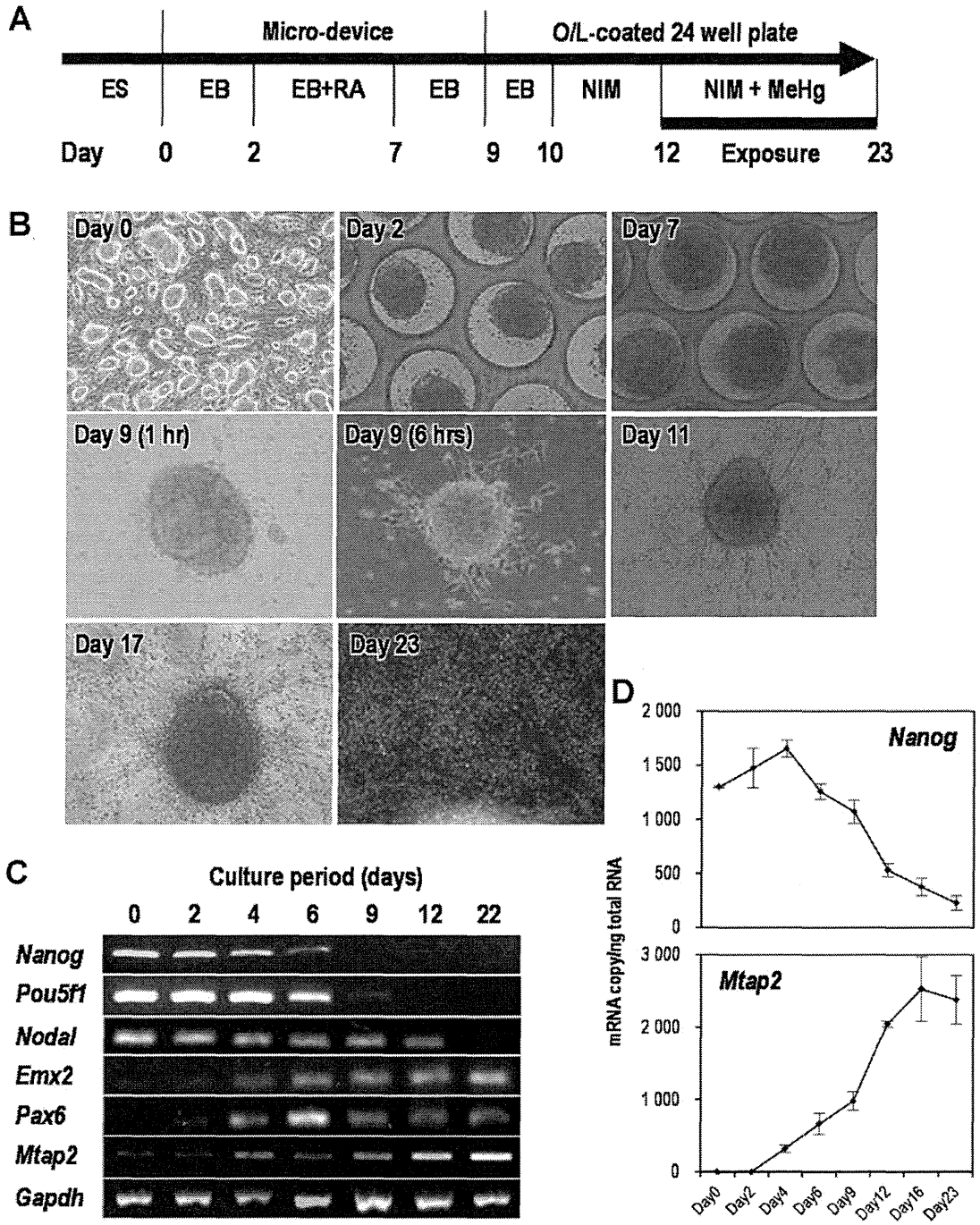

Fig. 1. Neuronal differentiation culture systems form mouse and human ESCs. (A and E) Schemesfor culture conditions and MeHg exposure using mESCs and hESCs (see details in Supplemental Materials, Methods). (B and F) Typical features of mESC and hESC colonies, mouse and human EBs growing in the micro-device, and differentiating neuronal cells. The values in parentheses are time after plating. Day 23 in mESCs and Day 50 in hESCs show MAP2 immunostaining, respectively. (C and G) Semi-quantitative RT-PCR analysis for differentiation marker genes. (D and H) Quantitative RT-PCR analysis for *Nanog*/*NANOG* and *Map2*/*MAP2* mRNAs. *Mtap2*/*MTAP2* is a official symbol of *Map2*/*MAP2*.

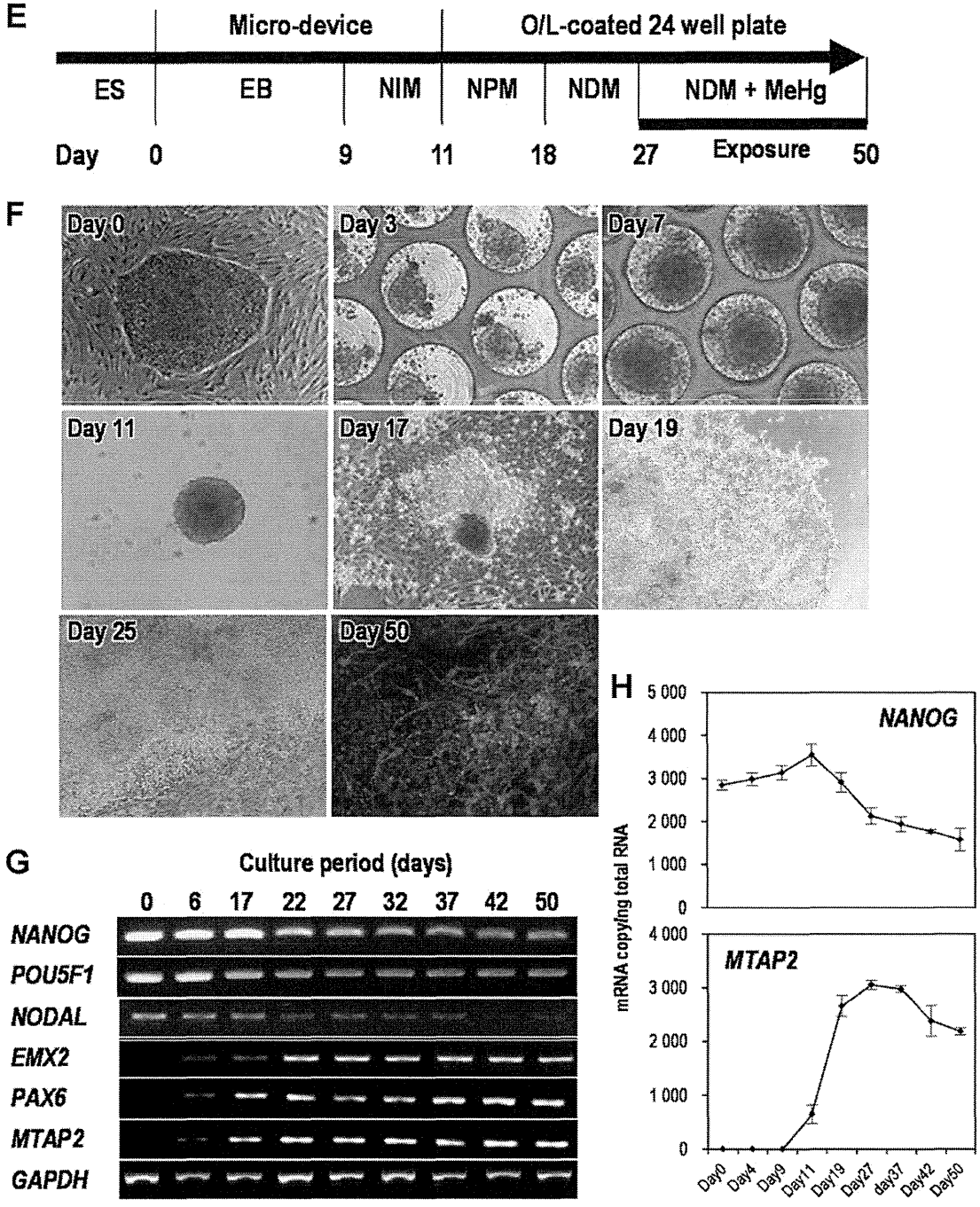

Fig. 1. (*Continued*).

3. Results

3.1. Neuronal differentiation of mESC and hESC derivatives

Typical features of neuronal differentiation from mESCs and hESCs are represented in Fig. 1B and F, respectively. In the mESC culture, EBs were generated in MSA and attached to O/L-coated dishes on Day 9. The migrating neuron-like cells appeared by Day 17. The *Nanog* mRNA level was decreased around Day 6 and became 17.3% at the end of culture (Fig. 1D). The neuronal lineage makers *Emx2*, *Pax6*, and *Map2* mRNAs were first detected on Day 4 and became stronger throughout neuronal induction (Fig. 1C). In contrast, the hESC derivatives continued to grow colonially and neuron-like cells appeared by Day 50 (Fig. 1F). In addition, *EMX2*, *PAX6*, and *MAP2* mRNAs were first detected around hESC-Day 17 (Fig. 1G), which was later compared with the mESC cultures (Fig. 1C). Although the *NANOG* mRNA was decreased around on Day 22, approximately one-half of the mRNAs were maintained till Day 50 (Fig. 1H).

3.2. Effects of MeHg on mESC and hESC derivatives cell viability

Based on the mRNA expression levels of neuronal differentiation markers, we considered that the mESC-Day 12 and the hESC-Day 27 cultures were similar stages of early neuronal development. MeHg exposure began on mESC-Day 12 and hESC-Day 27 and we measured the relative MTT activities compared with control (DMSO) for each time point (Fig. 2). The mESC-derived cells had completely disappeared within 5 days after the 1000 nM MeHg exposure (Fig. 2A),

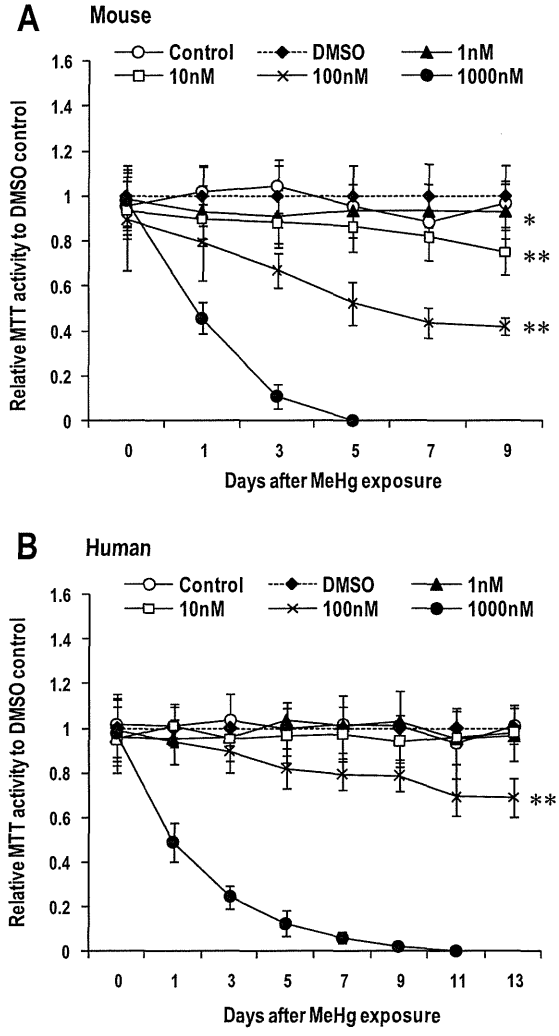

Fig. 2. Cytotoxicity of MeHg exposure to mESC- (A) and hESC-derived (B) neuronal cells. Serially diluted concentrations of MeHg were applied to the cells for the MTT assay (1, 10, 100 and 1000 nM). Cell viabilities for the DMSO control at each time point were used for normalization. Two-way ANOVA was used to determine the statistical difference (*$p < 0.05$; **$p < 0.01$).

whereas, it took 11 days for the same effect to be observed in the hESC derivatives (Fig. 2B). Significant decreases in mESCs cell viability were observed at 9 days after 1, 10 and 100 nM MeHg exposure. In contrast, we only observed a significant reduction in MTT activity in hESCs at 13 days after 100 nM MeHg exposure.

3.3. Effects of MeHg on morphologies of mESC and hESC derivatives

Typical MAP2-immunostainings at the end of the cell culturing period are shown in Fig. 3A and B. In mESC derivatives, the nuclear count was significantly decreased in the 100 nM group (0.16-fold) (Fig. 3C), and this result occurred from the drastic decrease in the viability of mESC derived cells (Fig. 2A). Conversely, significant differences in nuclear count were not found in the hESC derivatives (Fig. 3C). The Map2-positive neurite density from mESC derivatives was significantly decreased at the highest dose of MeHg (0.17-fold at 100 nM), whereas that of the hESCs was significantly decreased in all MeHg exposed groups (0.26-fold at 1 nM, 0.04-fold at 10 nM and 0.05-fold at 100 nM) (Fig. 3D). Furthermore, analysis of Map2-positive neurite lengths and branching points using ICA revealed that MeHg induced changes in morphological properties (Fig. 3E and F). With more details, significant reduce in Map2-positive neurite lengths was observed only at 100 nM group in mESC-derivatives (0.48-fold), while there was a significant dose-dependent decrease in neurite length in the hESCs, even at the lowest dose (Fig. 3E). The number of branching points in both mESC- and hESC-derivatives was only significantly reduced at 100 nM MeHg (0.54-fold and 0.65-fold, respectively) (Fig. 3F).

3.4. Effects of MeHg on the differentiation markers of mESC and hESC derivatives

Quantitative RT-PCR was performed at the end of the cell culturing period to investigate the effect of MeHg on the mRNA levels of the differentiation markers, especially those involved in central nervous system development. Although the mRNA copy numbers for the undifferentiated marker gene *Nanog* (mESC) and *NANOG* (hESC) were quite different from each other in control groups, they were increased by MeHg exposure (Fig. 4A and B). However, no significant increase in *Nanog* expression was observed in mESC-derivatives, while significant increases in *NANOG* expression were observed in 10 nM and 100 nM group in hESC-derivatives. For both mESC and hESC-derivatives, the TGFβ-family gene *NODAL* showed a definite tendency to be increased in a dose-dependent manner (Fig. 4A and B). However, significant increase was observed only in 100 nM group in hESC-derivatives. The neruroectoderm marker gene *PAX6* was significantly decreased by MeHg treatment in human cells in 10 nM and 100 nM groups (Fig. 4B). The mRNA levels of *EMX2* were also significantly deceased at the three doses in hESC-derivatives (Fig. 4B). The levels of the dendrite marker *MAP2* in both mESC and hESC-derivatives were significantly decreased at 100 nM MeHg. The expression of *Hoxb4* was significantly decreased in mESC-derivatives at 100 nM MeHg. Conversely, *HOXB4* showed significant dose-dependent upregulation in hESCs with the increasing concentrations of MeHg (Fig. 4B).

3.5. Network models

The interaction between MeHg exposure and gene expression levels observed in the PCR analyses was converted into network models using a Bayesian algorithm. In accordance with the principle of the previous reports (Friedman et al., 2000; Imoto et al., 2002), the regulatory effects of increasing amounts of chemical on mRNA levels can be evaluated in terms of a probabilistic inference. For mESC-derivatives, when *p*-value was defined over 0.5, the MeHg node dominated only five genes: *En1*, *Nodal*, *Nes*, *Otx1*, and *Hoxb1* (Fig. 5A). In hESC-derivatives, the MeHg node was located at the top of a network hierarchy and was related directly or indirectly to all the evaluated genes (Fig. 5B).

4. Discussion

The present study attempted to investigate the effects of MeHg in mESC- and hESC-derived neural developmental models using a combination of morphological and molecular markers. Numerous EBs of similar sizes were generated from both mESCs and hESCs using a unique micro-device (Sakai et al., 2010). With the exceptions of media, which was optimized for each culture, and differences in the MeHg exposure period, we attempted to adjust each protocol to be as similar to each other as possible. The concentrations of MeHg used to treat mESC and hESC in our study were 1,10,100 and 1000 nM, respectively. These concentrations are almost the same as levels detected in human whole blood (Grandjean et al., 1998).

The neuronal differentiation of hESCs generally requires a longer period than that of mESCs, which is likely due to the species-specific program. Watanabe and colleagues reported similar protocols for

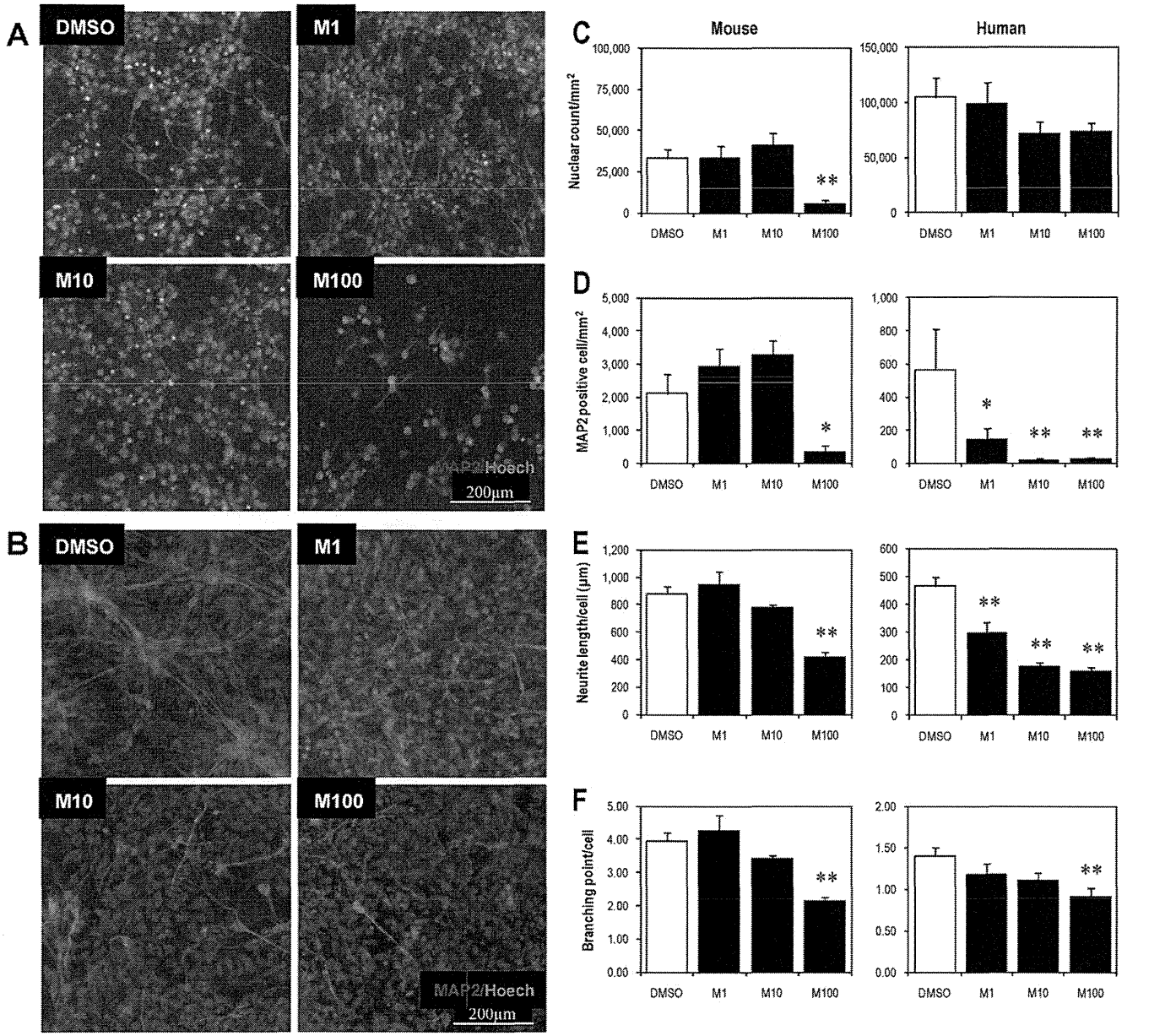

Fig. 3. The effect of MeHg exposure on the mESC- and hESC-derived neuronal cells. (A) Microphotographs of mESC neuronal derivatives on Day 23 (B) and hESC neural derivatives on Day 50. DMSO, control group; M1, 1 nM MeHg; M10, 10 nM of MeHg; M100, 100 nM of MeHg. Red: MAP2, blue: nucleus stained with Hoechst 33342. (C–F) Morphological measurement by high throughput automatic imaging analyzer (ICA) (see details in Supplemental Materials, Methods and Figs. S1 and S2). Data from 24-well culture plates were expressed as mean ± SE ($n = 6$). (C) Nuclear count per area. (D) MAP2-positive cell number per area. (E) Neurite length per cell. (F) Branching points per cell. One-way ANOVA followed by Fisher's PLSD test as post hoc were used to determine the statistical difference from DMSO control (*$p < 0.05$; **$p < 0.01$). (For interpretation of the references to color in this figure legend, the reader is referred to the web version of the article.)

the neuronal differentiation of mESCs and hESCs based on EB formation in serum-free suspension cultures (Eiraku et al., 2008; Watanabe et al., 2005, 2007). According to their reports, telencephalic precursors appeared within 5 days in the case of mESCs, whereas it took 35 days in the case of hESCs. Consistent with their reports, our study initially detected the expression of the neuronal marker genes on Day 4 in mESCs and on Day 17 in hESCs (Fig. 1C and G). At the end of culture, the mRNA copy numbers of *Map2* (mouse) on Day 23 and *MAP2* (human) on Day 50 were approximately equal, suggesting that the similar amounts of mature neural derivatives were successfully differentiated from both ESCs (Fig. 1D and H). In the morphological analysis, neuron proliferation was observed until Day 17 for mESC-derivatives, whereas the hESC-derivatives proliferated colonially in attached cultures on Day 42, and neuron proliferation was observed until Day 50 (Fig. 1B and 1E). These observations agree with previous studies that have examined the neuronal differentiation of both mESCs and hESCs (Nat et al., 2007; Song et al., 2008; Wada et al., 2009). Then, we exposed the cells to MeHg starting on Day 12 for mESCs and Day 27 for hESC because these times allowed for equivalent stages of development in both cell lines.

In utero exposure to MeHg causes severe neurodegenerative effects in human fetuses, which is known as congenital Minamata disease in Japan (Harada, 1978). In Iraq, neurodegenerative effects of MeHg have been attributed to the accidental ingestion of MeHg-contaminated wheat (Bakir et al., 1973). Whether human susceptibility to MeHg is greater than that of laboratory animals is not clear. According to the results of numerous *in vitro* studies using neuronal cell-lines of rodents and human, there is a tendency for human cells to be more susceptible to MeHg

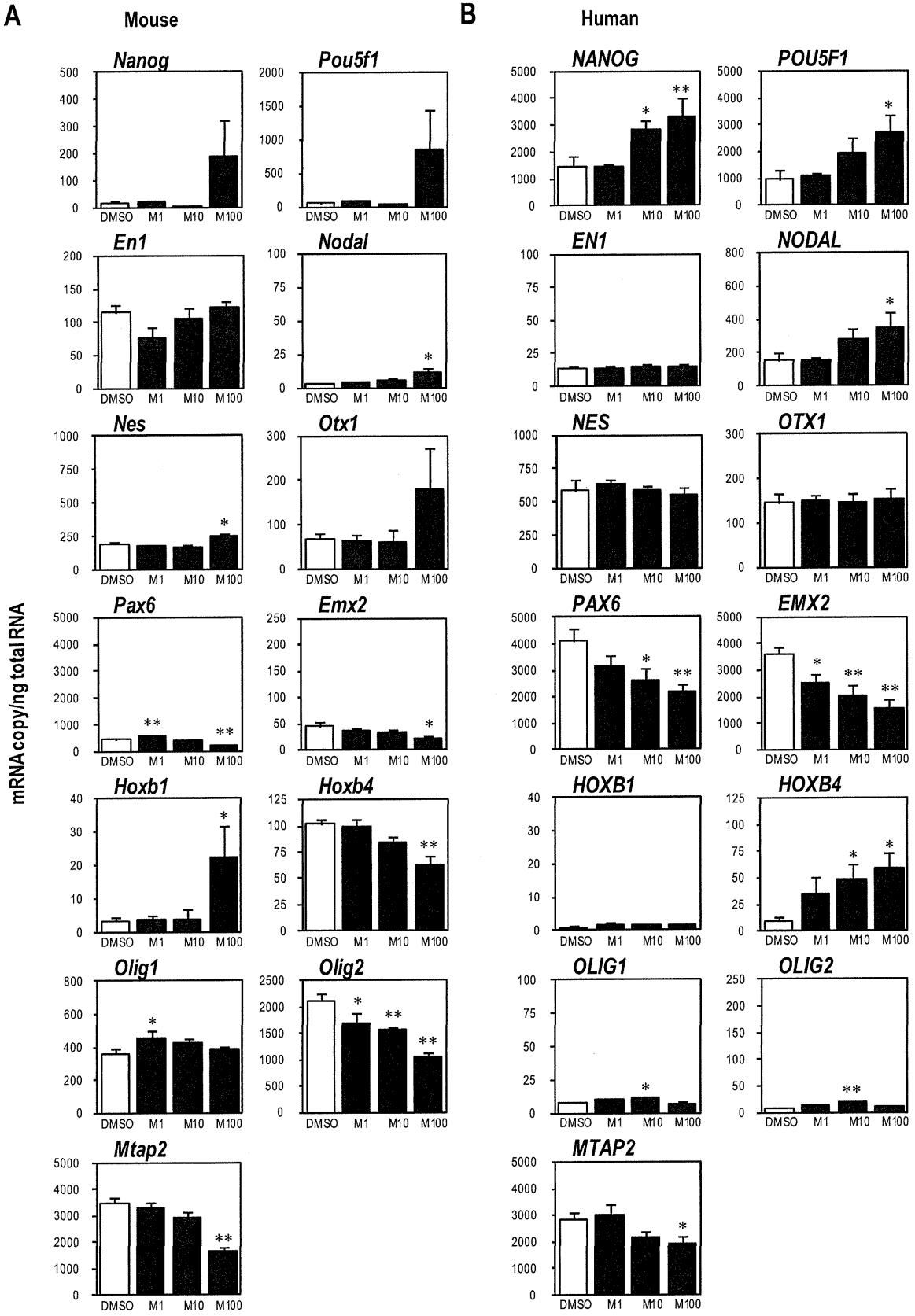

Fig. 4. The effect of MeHg exposure on the gene expression in mESC (A) and hESC (B) derivatives at the end of culture. Expression levels were calculated as absolute copy numbers of target mRNAs per total RNA. Data from 24-well culture plates were expressed as mean ± SE ($n = 6$). DMSO, control group; M1, 1 nM of MeHg; M10, 10 nM of MeHg; M100, 100 nM of MeHg. One-way ANOVA followed by Fisher's PLSD test as post hoc were used to determine the statistical difference from DMSO control (*$p < 0.05$; **$p < 0.01$).

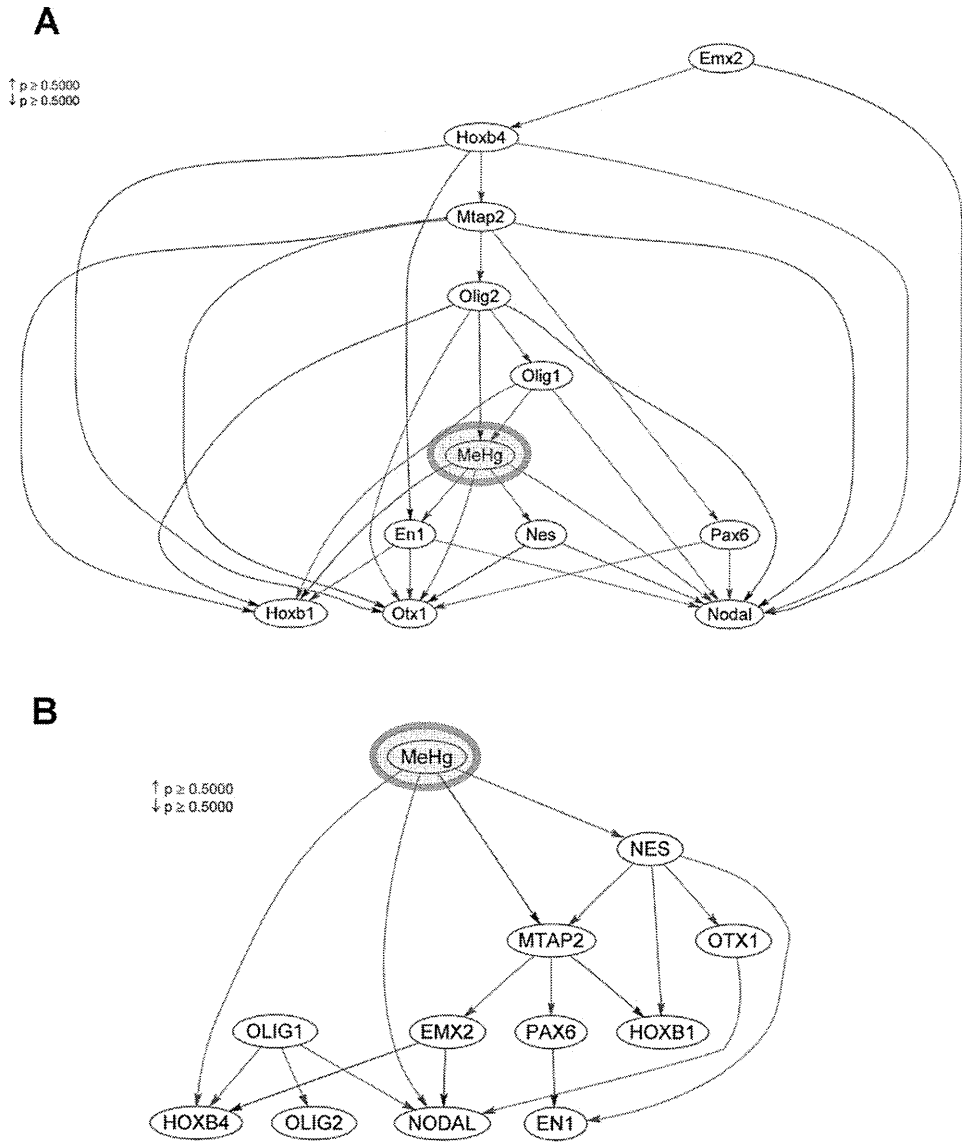

Fig. 5. Bayesian network models for the effect of MeHg exposure on the mESC (A) and hESC (B) derivatives. Correlations among chemical concentrations (MeHg: red circle) and gene expression levels (11 genes) were analyzed and drawn automatically by a computer software. The β-value of the Bayesian model was expressed as a red arrow if positively relative, and a blue arrow if negatively relative. The correlation probability ($p > 0.05$) was defined in the analysis. (For interpretation of the references to color in this figure legend, the reader is referred to the web version of the article.)

poisoning (Ceccatelli and Moors, 2010). Some of the behavioral effects of MeHg in rodents remain controversial, and the methods for modeling human MeHg exposure in animals require further optimization (Liang et al., 2009). For example, in a murine prenatal exposure model, MeHg (31.9 nmol/g food) accumulated at approximately 25 μg/g fetal brain and resulted in approximately 40% total embryonic/fetal death (Satoh and Suzuki, 1983). Interestingly, other than subtle defects in working memory, visual spatial ability, and anxiety-like behavior, no neurological defects were detected following the accumulation of 12.8–13.3 μg/g brain of mice (Liang et al., 2009). In human epidemiological studies, the highest level of MeHg in umbilical cords from the patients with congenital Minamata disease was 1.60 ± 1.00 ppm (Harada et al., 1999). Although it is difficult to comment on interspecies differences using previous published studies, taken together, they suggest that human susceptibility to MeHg is greater than that of mice, particularly with regard to the functional status of developing neurons. In this present study, our cytotoxicity assays and morphological analyses provided possible, but limited, evidences that cell death in immature mouse neuronal cells occurs at lower doses of MeHg than that in humans, although the morphology and functional status of the surviving cells remain normal. In contrast, the abnormal differentiation and maturation of neurons in humans may begin at lower concentrations of MeHg than those required for cell death, which could result in neuro-performance symptoms in infants. However, it should be noted that the density of Map2-positive cells was different between our mESC and hESC models, which might also affect their sensitivities to MeHg exposure.

In our study, the reductions in gene expression levels for *PAX6* and *EMX2* were clearly detected in hESC-derivatives exposed to low doses of MeHg. On the other hand, the deletion or mutation of *Pax6* or *Emx2* in mice has been reported to cause severe cortical dysplasia in mouse (Caric et al., 1997; Mallamaci et al., 2000). Furthermore, a human genetic study showed that the *PAX6* gene had a dosage effect in a family with congenital cataracts, aniridia, anophthalmia and central nervous system defects (Glaser et al., 1994). These suggest that both *PAX6* and *EMX2* genes may cooperate in the proliferation and differentiation of neuronal stem cells

and the migration of neuronal progenitors during the formation of the cerebral cortex in the fetus.

Bayesian network analysis has been reported to predict gene interaction networks and protein-protein interactions (Friedman et al., 2000; Imoto et al., 2002; Jansen et al., 2003; Pe'er et al., 2001). The Bayesian network is drawn as a directed acyclic graph, having a direction with a hierarchy in which a parent node affects the child node(s). Therefore elements that exert more effects should be located higher in the hierarchy of a calculated network model. In the toxicological studies, Bayesian network analysis has been used to map the dose-dependent response of biomarkers to chemical exposures (Hack et al., 2010; Nagano et al., 2012; Yang et al., 2010). According to our analysis of mESC-derived cells, the node for MeHg was located to the middle of hierarchy, which suggested that MeHg toxicity could not be more definitively mapped because of the slight effects at lower doses. In contrast, the node for MeHg in hESCs was located to the top of network hierarchy, which suggested that MeHg affects the differentiation of neuronal cells in hESCs more significantly than it does in the mESCs, although differences between these two culture systems, such as the time frame of the neuronal differentiation process, length of exposure, and composition of the culture media, should also be taken into consideration (Fig. 5B).

The EST endorsed by ECVAM includes a cytotoxicity assay and a cardiac differentiation inhibition assay using mESC cells. Twenty test chemicals with known *in vivo* embryo toxic potential, including MeHg, were tested in blind conditions, and good reproducibility was achieved (*i.e.*, an accuracy of 78%) (Genschow et al., 2004). MeHg exposure studies in a mESC neuronal differentiation system found an IC_{50} value of 260 nM using resazurin cytotoxicity test of 14 days continuous exposure (Stummann et al., 2007). Consistent with our study, there was a decrease in *Map2* mRNA expression at 100 nM, which was a non-cytotoxic concentration (Stummann et al., 2007). The hESC neuronal differentiation system has been also used to test the embryo toxic potential of MeHg by the same research team (Stummann et al., 2009). Following 12 days continuous exposure (cytotoxicity, IC_{50} value = 39 nM), the neuronal marker genes *NEUROD1* and *MAP2* showed significant decreases of 55% and 29%, respectively, in the presence of 25 nM MeHg. Although the cytotoxicity data for mESCs were different from the present data, the data from hESCs were similar. In addition to significant reductions in the expression of *PAX6* and *EMX2* at MeHg exposure levels less than 10 nM, there was a tendency for a reduction of *MAP2* expression, which suggested a consistent dose-response for human neuronal development.

Human neuronal precursor cells (hNPC) can be used as an alternative model to test human susceptibility to developmental neurotoxicants (Moors et al., 2009). An hNPC can differentiate into neurons in approximately one week, which is an advantage over human ESTs. Based on the ratio of hNPC derived Tuj1-positive neuron and migration activity, more than 500 nM of MeHg showed toxic effect (Moors et al., 2009), which suggests a much higher level of resistance than that observed in the present study. This large difference may be due to the different differentiation states of hNPCs at the time of MeHg exposure compared with those of human neuronal progenitors from ESCs. Indeed, the progenitors produced in our culture system (Day 27) may have been more immature, which could have increased their sensitivity to MeHg. Despite continuous exposure for an extended time (23 days), the present results showed that differentiated MAP2-positive neuronal cells were able to survive (Fig. 3B). This observation indicated that mature neuronal cells are more resistant to MeHg than immature cells. Therefore, ESTs appear to evaluate embryo toxicity more effectively than an hNPC culture system. For example, the critical window for observing psychiatric defects (*e.g.*, autism spectrum disorder) as a result of thalidomide exposure is suspected to occur before 25 days of postfertilization (Miller et al., 2005). The effects of chemicals such as thalidomide on earlier stages can only be analyzed with ESTs, which clearly highlights the advantages of human ESTs over hNPCs.

In summary, we examined the effects of MeHg in a low concentration range of 1–1000 nM on the neural differentiation of mESCs and hESCs using a battery of tests, including cell viability assay, morphological and molecular assessments, and network analysis. Our study provided possible, but limited, evidences that human ESC models might be more sensitive in particular endpoints in response to MeHg exposure than that in mouse ESC models. Further investigations that expand on the findings of the present paper may solve problems that occur when the outcomes from laboratory animals are extrapolated for human risk evaluation.

Conflict of interest statement

The authors declare that they have no competing financial interests.

Acknowledgments

This study was supported in part by the Environmental Technology Development Fund (to H. S.) from the Ministry of the Environment and the Grant in Aid for Scientific Research from the Ministry of the Health and Labor (to S. O.), Japan. The authors gratefully acknowledge the technical support of Miss Noriko Oshima (GE Healthcare Japan Corporation) in the analysis using IN Cell Analyzer 1000 and Dr Shigeru Koikegami (Second Lab, LLC) in constructing software for a Bayesian algorithm. The authors also thank Miss Masami Yokoyama for her technical assistance.

Appendix A. Supplementary data

Supplementary data associated with this article can be found, in the online version, at http://dx.doi.org/10.1016/j.toxlet.2012.04.011.

References

Airaksinen, R., Turunen, A.W., Rantakokko, P., Mannisto, S., Vartiainen, T., Verkasalo, P.K., 2010. Blood concentration of methylmercury in relation to food consumption. Public Health Nutrition 14, 480–489.

Baek, D.H., Kim, T.G., Lim, H.K., Kang, J.W., Seong, S.K., Choi, S.E., Lim, S.Y., Park, S.H., Nam, B.H., Kim, E.H., Kim, M.S., Park, K.L., 2011. Embryotoxicity assessment of developmental neurotoxicants using a neuronal endpoint in the embryonic stem cell test. Journal of Applied Toxicology, http://dx.doi.org/10.1002/jat. 1747.

Bakir, F., Damluji, S.F., Amin-Zaki, L., Murtadha, M., Khalidi, A., al-Rawi, N.Y., Tikriti, S., Dahahir, H.I., Clarkson, T.W., Smith, J.C., Doherty, R.A., 1973. Methylmercury poisoning in Iraq. Science 181, 230–241.

Brend, T., Gilthorpe, J., Summerbell, D., Rigby, P.W., 2003. Multiple levels of transcriptional and post-transcriptional regulation are required to define the domain of Hoxb4 expression. Development 130, 2717–2728.

Caric, D., Gooday, D., Hill, R.E., McConnell, S.K., Price, D.J., 1997. Determination of the migratory capacity of embryonic cortical cells lacking the transcription factor Pax-6. Development 124, 5087–5096.

Ceccatelli, S., Daré, E., Moors, M., 2010. Methylmercury-induced neurotoxicity and apoptosis. Chemico-Biological Interactions 188, 301–308.

Choi, B.H., 1989. The effects of methylmercury on the developing brain. Progress in Neurobiology 32, 447–470.

Davidson, P.W., Myers, G.J., Weiss, B., 2004. Mercury exposure and child development outcomes. Pediatrics 113, 1023–1029.

Duparc, R.H., Boutemmine, D., Champagne, M.P., Tetreault, N., Bernier, G., 2006. Pax6 is required for delta-catenin/neurojugin expression during retinal, cerebellar and cortical development in mice. Developmental Biology 300, 647–655.

Eiraku, M., Watanabe, K., Matsuo-Takasaki, M., Kawada, M., Yonemura, S., Matsumura, M., Wataya, T., Nishiyama, A., Muguruma, K., Sasai, Y., 2008. Self-organized formation of polarized cortical tissues from ESCs and its active manipulation by extrinsic signals. Cell Stem Cell 3, 519–532.

Friedman, N., Linial, M., Nachman, I., Pe'er, D., 2000. Using Bayesian networks to analyze expression data. Journal of Computational Biology 7, 601–620.

Galli, R., Fiocco, R., De Filippis, L., Muzio, L., Gritti, A., Mercurio, S., Broccoli, V., Pellegrini, M., Mallamaci, A., Vescovi, A.L., 2002. Emx2 regulates the proliferation of stem cells of the adult mammalian central nervous system. Development 129, 1633–1644.

Genschow, E., Spielmann, H., Scholz, G., Pohl, I., Seiler, A., Clemann, N., Bremer, S., Becker, K., 2004. Validation of the embryonic stem cell test in the international ECVAM validation study on three in vitro embryotoxicity tests. Alternatives to Laboratory Animal 32, 209–244.

Glaser, T., Jepeal, L., Edwards, J.G., Young, S.R., Favor, J., Maas, R.L., 1994. PAX6 gene dosage effect in a family with congenital cataracts, aniridia, anophthalmia and central nervous system defects. Nature Genetics 7, 463–471.

Grandjean, P., Weihe, P., White, R.F., Debes, F., 1998. Cognitive performance of children prenatally exposed to safe levels of methylmercury. Environmental Research 77 (May (2)), 165–172.

Grandjean, P., Satoh, H., Murata, K., Eto, K., 2010. Adverse effects of methylmercury: environmental health research implications. Environmental Health Perspectives 118, 1137–1145.

Hack, C.E., Haber, L., Maier, A., Shulte, P., Fowler, B., Lotz, W.G., Savage Jr., R.E., 2010. A Bayesian network model for biomarker-based dose response. Risk Analysis 30, 1037–1051.

Harada, M., 1978. Congenital Minamata disease: intrauterine methylmercury poisoning. Teratology 18, 285–288.

Harada, M., Akagi, H., Tsuda, T., Kizaki, T., Ohno, H., 1999. Methylmercury level in umbilical cords from patients with congenital Minamata disease. Science of the Total Environment 234, 59–62.

Hu, G.Q., Jin, M.H., Lin, X.L., Guo, C.X., Zhang, L., Sun, Z.W., 2010. Mercury distribution in neonatal rat brain after intrauterine methylmercury exposure. Environmental Toxicology and Pharmacology 29, 7–11.

Imoto, S., Goto, T., Miyano, S., 2002. Estimation of genetic networks and functional structures between genes by using Bayesian networks and nonparametric regression. Pacific Symposium on Biocomputing 7, 175–186.

Jansen, R., Yu, H., Greenbaum, D., Kluger, Y., Krogan, N.J., Chung, S., Emili, A., Snyder, M., Greenblatt, J.F., Gerstein, M., 2003. A Bayesian networks approach for predicting protein-protein interactions from genomic data. Science 302, 449–453.

Kuntz, S.W., Ricco, J.A., Hill, W.G., Anderko, L., 2010. Communicating methylmercury risks and fish consumption benefits to vulnerable childbearing populations. Journal of Obstetric, Gynecologic, and Neonatal Nursing 39, 118–126.

Liang, J., Inskip, M., Newhook, D., Messier, C., 2009. Neurobehavioral effect of chronic and bolus doses of methylmercury following prenatal exposure in C57BL/6 weanling mice. Neurotoxicology and Teratology 31, 372–381.

Mallamaci, A., Mercurio, S., Muzio, L., Cecchi, C., Pardini, C.L., Gruss, P., Boncinelli, E., 2000. The lack of Emx2 causes impairment of Reelin signaling and defects of neuronal migration in the developing cerebral cortex. Journal of Neuroscience 20, 1109–1118.

Miller, M.T., Stromland, K., Ventura, L., Johansson, M., Bandim, J.M., Gillberg, C., 2005. Autism associated with conditions characterized by developmental errors in early embryogenesis: a mini review. International Journal of Developmental Neuroscience: the Official Journal of the International Society for Developmental Neuroscience 23, 201–219.

Moors, M., Rockel, T., Abel, J., Cline, J.E., Gassmann, K., Schreiber, T., Schuwald, J., Weinmann, N., Fritsche, E., 2009. Human neurospheres as three-dimensional cellular systems for developmental neurotoxicity testing. Environmental Health Perspectives 117, 1131–1138.

Murabe, M., Yamauchi, J., Fujiwara, Y., Hiroyama, M., Sanbe, A., Tanoue, A., 2007. A novel embryotoxic estimation method of VPA using ES cells differentiation system. Biochemical and Biophysical Research Communications 352, 164–169.

Nagano, R., Akanuma, H., Qin, X.Y., Imanishi, S., Toyoshiba, H., Yoshinaga, J., Ohsako, S., Sone, H., 2012. Multi-parametric profiling network based on gene expression and phenotype data: a novel approach to developmental neurotoxicity testing. International Journal of Molecular Sciences 13, 187–207.

Nat, R., Nilbratt, M., Narkilahti, S., Winblad, B., Hovatta, O., Nordberg, A., 2007. Neurogenic neuroepithelial and radial glial cells generated from six human embryonic stem cell lines in serum-free suspension and adherent cultures. Glia 55, 385–399.

Pe'er, D., Regev, A., Elidan, G., Friedman, N., 2001. Inferring subnetworks from perturbed expression profiles. Bioinformatics 17 (Suppl. 1), S215–S224.

Reubinoff, B.E., Pera, M.F., Fong, C.Y., Trounson, A., Bongso, A., 2000. Embryonic stem cell lines from human blastocysts: somatic differentiation in vitro. Nature Biotechnology 18, 399–404.

Sakai, Y., Yoshida, S., Yoshiura, Y., Mori, R., Tamura, T., Yahiro, K., Mori, H., Kanemura, Y., Yamasaki, M., Nakazawa, K., 2010. Effect of microwell chip structure on cell microsphere production of various animal cells. Journal of Bioscience and Bioengineering 110, 223–229.

Sakata, Y., Yoshioka, W., Tohyama, C., Ohsako, S., 2007. Internal genomic sequence of human CYP1A1 gene is involved in superinduction of dioxin-induced CYP1A1 transcription by cycloheximide. Biochemical and Biophysical Research Communications 355, 687–692.

Satoh, H., Suzuki, T., 1983. Embryonic and fetal death after in utero methylmercury exposure and resultant organ mercury concentrations in mice. Industrial Health 21, 19–24.

Shimizukawa, R., Sakata, A., Hirose, M., Takahashi, A., Iseki, H., Liu, Y., Kunita, S., Sugiyama, F., Yagami, K., 2005. Establishment of a new embryonic stem cell line derived from C57BL/6 mouse expressing EGFP ubiquitously. Genesis 42, 47–52.

Song, T., Chen, G., Wang, Y., Mao, G., Bai, H., 2008. Chemically defined sequential culture media for TH+ cell derivation from human embryonic stem cells. Molecular Human Reproduction 14, 619–625.

Stummann, T.C., Bremer, S., 2008. The possible impact of human embryonic stem cells on safety pharmacological and toxicological assessments in drug discovery and drug development. Current Stem Cell Research & Therapy 3, 118–131.

Stummann, T.C., Hareng, L., Bremer, S., 2007. Embryotoxicity hazard assessment of methylmercury and chromium using embryonic stem cells. Toxicology 242, 130–143.

Stummann, T.C., Hareng, L., Bremer, S., 2009. Hazard assessment of methylmercury toxicity to neuronal induction in embryogenesis using human embryonic stem cells. Toxicology 257, 117–126.

Suemori, H., Yasuchika, K., Hasegawa, K., Fujioka, T., Tsuneyoshi, N., Nakatsuji, N., 2006. Efficient establishment of human embryonic stem cell lines and long-term maintenance with stable karyotype by enzymatic bulk passage. Biochemical and Biophysical Research Communications 345, 926–932.

Tada, S., Era, T., Furusawa, C., Sakurai, H., Nishikawa, S., Kinoshita, M., Nakao, K., Chiba, T., 2005. Characterization of mesoendoderm: a diverging point of the definitive endoderm and mesoderm in embryonic stem cell differentiation culture. Development 132, 4363–4374.

Tamm, C., Duckworth, J., Hermanson, O., Ceccatelli, S., 2006. High susceptibility of neural stem cells to methylmercury toxicity: effects on cell survival and neuronal differentiation. Journal of Neurochemistry 97, 69–78.

Theunissen, P.T., Pennings, J.L., Robinson, J.F., Claessen, S.M., Kleinjans, J.C., Piersma, A.H., 2011. Time-response evaluation by transcriptomics of methylmercury effects on neural differentiation of murine embryonic stem cells. Toxicological Sciences 122, 437–447.

Thomson, J.A., Itskovitz-Eldor, J., Shapiro, S.S., Waknitz, M.A., Swiergiel, J.J., Marshall, V.S., Jones, J.M., 1998. Embryonic stem cell lines derived from human blastocysts. Science 282, 1145–1147.

Toyoshiba, H., Yamanaka, T., Sone, H., Parham, F.M., Walker, N.J., Martinez, J., Portier, C.J., 2004. Gene interaction network suggests dioxin induces a significant linkage between aryl hydrocarbon receptor and retinoic acid receptor beta. Environmental Health Perspectives 112, 1217–1224.

Wada, T., Honda, M., Minami, I., Tooi, N., Amagai, Y., Nakatsuji, N., Aiba, K., 2009. Highly efficient differentiation and enrichment of spinal motor neurons derived from human and monkey embryonic stem cells. PLoS One 4, e6722.

Watanabe, K., Kamiya, D., Nishiyama, A., Katayama, T., Nozaki, S., Kawasaki, H., Watanabe, Y., Mizuseki, K., Sasai, Y., 2005. Directed differentiation of telencephalic precursors from embryonic stem cells. Nature Neuroscience 8, 288–296.

Watanabe, K., Ueno, M., Kamiya, D., Nishiyama, A., Matsumura, M., Wataya, T., Takahashi, J.B., Nishikawa, S., Nishikawa, S., Muguruma, K., Sasai, Y., 2007. A ROCK inhibitor permits survival of dissociated human embryonic stem cells. Nature Biotechnology 25, 681–686.

Weiss, B., Stern, S., Cox, C., Balys, M., 2005. Perinatal and lifetime exposure to methylmercury in the mouse: behavioral effects. Neurotoxicology 26, 675–690.

Yang, X., Zhang, B., Molony, C., Chudin, E., Hao, K., Zhu, J., Gaedigk, A., Suver, C., Zhong, H., Leeder, J.S., Guengerich, F.P., Strom, S.C., Schuetz, E., Rushmore, T.H., Ulrich, R.G., Slatter, J.G., Schadt, E.E., Kasarskis, A., Lum, P.Y., 2010. Systematic genetic and genomic analysis of cytochrome P450 enzyme activities in human liver. Genome Research 20, 1020–1036.

Supplemental Material

Effects of Methylmercury Exposure on Neuronal Differentiation of Mouse and Human Embryonic Stem Cells

Xiaoming He, Satoshi Imanishi, Hideko Sone, Reiko Nagano, Xian-Yang Qin, Jun Yoshinaga, Hiromi Akanuma, Junko Yamane, Wataru Fujibuchi, Seiichiroh Ohsako

Contents

Supplemental Methods

Reagents.

Dullbecco's Modified Eagle's Medium (D-MEM) (1X) without phenol red, D-MEM/F-12 (1X) liquid 1:1 without phenol red, Neurobasal® Medium (1X) without phenol red, ES cell qualified fetal bovine serum (FBS), Knockout™ Serum Replacement (KSR), N-2 Supplement (100X), B-27® Supplement Minus Vitamin A (50X), recombinant human brain-derived neurotrophic factor (BDNF), GlutaMAX™-I (100X), MEM Non-Essential Amino Acids Solution 10 mM (100X) (NEAA), TrypLE™ Select, Penicillin-Streptomycin (5,000 units/ml, 5,000μg/ml), 2-Mercaptoethanol (55 mM in D-PBS, 1000X) (2-ME), and Alexa568-conjugated rabbit anti-mouse IgG were purchased from Invitrogen Corporation (Carlsbad, CA). Gelatin from porcine skin type A, Poly-L-ornithine solution 0.01%, Laminin from Engelbreth-Holm-Swarm murine sarcoma basement membrane, methylmercury chloride (II) (MeHg), and mouse monoclonal anti-MAP2 antibody were purchased from Sigma-Aldrich (St. Louis, MO). Recombinant human basic-FGF (bFGF), all-trans retinoic acid (RA), and ROCK inhibitor Y-27632 were purchased from Wako Pure Chemical Industries (Chuo-ku, Osaka, Japan). Dimethyl sulfoxide (DMSO) and MTT cell-number counting kit (MTT-Assay Kit) were purchased from Nacalai Tesque, Inc. (Nakagyo-ku, Kyoto, Japan). Murine recombinant leukemia inhibitory factor (mLIF, ESGRO®) was purchased from Millipore (Billerica, MA). Hoechst 33342 solution was purchased from Dojindo Laboratories (Kumamoto, Japan). The RNeasy Mini kit was purchased from QIAGEN (Hilden, Germany). LightCycler® 480 SYBR Green I Master was purchased from Roche Diagnostics GmbH (Mannheim, Germany). The PrimeScript® RT reagent Kit and TaKaRa Ex-Taq were purchased from Takara BIO Inc. (Otsu, Shiga, Japan). All oligonucleotides purified by gel-filtration were purchased from Hokkaido System Science (Sapporo, Hokkaido, Japan).

Culture and neuronal differentiation of mouse embryonic stem cells.

The mESC line, B6G-2 (XY genotype), was maintained in the medium composed of D-MEM containing 15% FBS, 100 μM NEAA, 55 μM 2-ME, and 1,000 U/ml mLIF. Mouse ESCs were cultured on feeder cells of mouse embryonic fibroblasts (MEFs), which were plated on 0.1% gelatin-coated dish. They were re-plated onto 60 mm dishes twice without additional MEFs. The mESCs were harvested at 48 hrs after the last passage (purity > 99%) and suspended in the medium containing D-MEM, 15% KSR, 100 μM NEAA, and 55 μM 2-ME (EB-medium). The suspended mESCs were dissociated into single cells by mechanical pipetting, seeded at 2.0×10^5 cells onto the culture device of a microsphere array (MSA; 1020 holes, φ300 μm/hole, STEM